

# A Comparison of Relativistic Coupled Cluster and Equation of Motion Coupled Cluster Quadratic Response Theory

Xiang Yuan,<sup>†,‡</sup> Loïc Halbert,<sup>†</sup> Lucas Visscher,<sup>¶</sup> and André Severo Pereira  
Gomes<sup>\*,†</sup>

<sup>†</sup>*Univ. Lille, CNRS, UMR 8523 - PhLAM - Physique des Lasers Atomes et Molécules,  
F-59000 Lille, France*

<sup>‡</sup>*Department of Chemistry and Pharmaceutical Sciences, Faculty of Science, Vrije  
Universiteit Amsterdam, 1081 HV Amsterdam, The Netherlands*

<sup>¶</sup>*Department of Chemistry and Pharmaceutical Sciences, Faculty of Science, Vrije  
Universiteit Amsterdam, 1081 HZ Amsterdam, The Netherlands*

E-mail: andre.gomes@univ-lille.fr

## Abstract

We present the implementation of relativistic coupled cluster quadratic response theory (QR-CC), following our development of relativistic equation of motion coupled cluster quadratic response theory (QR-EOMCC) [X. Yuan *et al.*, *J. Chem. Theory Comput.* 2023, **19**, 9248]. These codes, which can be used in combination with relativistic (2- and 4-component based) as well as non-relativistic Hamiltonians, are capable of treating both static and dynamic perturbations for electric and magnetic operators. We have employed this new implementation to revisit the calculation of static and frequency-dependent first hyperpolarizabilities of hydrogen halides (HX, X=F-Ts) and

the Verdet constant of heavy noble gas atoms (Xe, Rn, Og), in order to investigate the differences and similarities of QR-CC and the more approximate QR-EOMCC. Furthermore, we have determined the relative importance of scalar relativistic effects and spin-orbit coupling to these properties, through a comparison of different Hamiltonians, and extended our calculations to superheavy element species (HTs for hyperpolarizabilities, Og for the Verdet constant). Our results show that as one moves towards the bottom of the periodic table, QR-EOMCC can yield rather different results (hyperpolarizabilities) or perform rather similarly (Verdet constant) to QR-CC. These results underscore the importance of further characterizing the performance of QR-EOMCC for heavy element systems.

## Introduction

External perturbations such as those induced by electric or magnetic fields allow us to probe the electronic structure of atoms, molecules and materials, with different perturbations providing us with complementary information about the system.<sup>1,2</sup> The first-order (linear) responses to such a perturbation are particularly sought-after quantities, since from them one can obtain information about electronically or vibrationally<sup>3</sup> excited states through processes involving a single photon, or magnetic properties such as NMR shieldings or indirect spin-spin coupling constants<sup>4-6</sup> to name but a few.

Properties arising from the interaction with two or more photons<sup>7,8</sup> at a time are also of great interest be it for technological applications in non-linear optics<sup>9,10</sup> or for speciation through two-photon absorption,<sup>11</sup> as the differences in selection rules compared to one-photon processes allow for probing different states.

Theoretical models are indispensable to interpret experimental results, and the last fifty years have seen the development<sup>12,13</sup> of approaches based on *ab initio* molecular electronic structure theory gain popularity in applications, thanks in no small part to the development of response theory<sup>2,14,15</sup> and its application to different models such as multi-configurational

self-consistent field theory,<sup>16-18</sup> density functional theory,<sup>19</sup> and coupled cluster theory.<sup>20-22</sup> The use of the time-averaged quasienergy formalism<sup>21,23-35</sup> has provided not only a unified framework, with which to derive response for both variational and non-variational approaches, but also a way to enable the development of embedding approaches in which variational and non-variational electronic structure methods are combined<sup>36-43</sup> to calculate molecular properties in large systems within a fully quantum mechanical description in a cost-effective manner.

In the case of coupled cluster theory, one can identify two main approaches, one which employs an exponential parametrization for the time evolution of the cluster operators (CC response), and another based on the equation of motion formalism (EOMCC response)<sup>44-53</sup> for which a linear parametrization is employed to obtain molecular properties.

From the outset, key differences between the two approaches have been identified with respect to separability,<sup>21,54,55</sup> with as consequence that CC transition moments are size-extensive whereas EOMCC ones are not. More recently the interconnections between these two approaches were further investigated from a formal point of view.<sup>56,57</sup>

In spite of such differences, the calculation of response properties within the EOMCC formalism remains appealing from both the implementation and the application points of view,<sup>58-60</sup> as simplifications in the equations also translate into a somewhat more modest computational cost. This calls for an understanding of how the two approaches differ in practical calculations. In the literature comparisons between linear response CC (LR-CC) and EOMCC (LR-EOMCC) properties<sup>49,50,57,61</sup> so far suggest that, in spite of the lack of size-extensivity of EOM-CC transition moments, in practice the two approaches yield quite similar results.

Similar conclusions have been reached when comparing quadratic response CC (QR-CC) and EOMCC (QR-EOMCC) results for dipole hyperpolarizabilities,<sup>46,48,57</sup> though comparisons were initially limited to a few systems. More recently, an extensive benchmark study on excited state transition moments,<sup>62</sup> which also probe quadratic response functions, seem

to confirm the tendencies observed previously. These previous evaluations were carried out for valence properties of molecules containing light elements, that is, occupying the first two rows of the periodic table. For properly representing the molecular properties of heavier systems it is necessary to account for relativistic effects<sup>63-69</sup> and to the best of our knowledge there is currently no data in the literature assessing the differences between the two approaches beyond the second row of the periodic table.

Response theory can be used in combination with relativistic Hamiltonians,<sup>70</sup> and implementations for mean-field approaches (Hartree-Fock and DFT) are for example available for the calculation of frequency-dependent linear and non-linear response properties for 4-component-based Hamiltonians.<sup>71-81</sup> To go beyond mean-field, relativistic coupled cluster theory<sup>82-87</sup> offers a flexible framework for obtaining accurate energies and properties which treats electron correlation and relativistic effects on the same footing. It can thereby be used to investigate systems of interest across the periodic table, and benchmark more approximate methods.

In recent years there have been extensive efforts by different groups to address states beyond closed-shell ground states through EOMCC theory for excitation and ionization energies, and electron affinities.<sup>88-103,103-112</sup> While some of these implementations allow for the calculation of transition moments or static properties (through the application of finite fields or via approximate expectation values), full-fledged implementations of CC or EOMCC response theory are much more scarce. Yuan et al.<sup>113</sup> have reported an implementation capable of carrying out frequency-dependent LR-CC and LR-EOMCC calculations for different (from 1- to 4-component based) Hamiltonians for electric, magnetic and mixed electric-magnetic properties. A comparison of CC and EOMCC showed that for dipole polarizabilities the two approaches do yield similar results as relativistic effects become more pronounced, but for indirect spin-spin coupling constants there is growing difference between the two. Chakraborty et al.<sup>114</sup> reported an efficient implementation of LR-CC for the spin-free eXact 2-Component Hamiltonian (x2C) and applied it to investigate the static and dynamic dipole polarizabilities

of an extensive set of molecular systems.

Beyond linear response, the analytical treatment of quadratic response coupled cluster theory would be particularly useful in applications in which finite field calculations are not straightforward, easy to converge or inapplicable, such for frequency-dependent calculations of non-linear optical properties or in the study of birefringences. However, general implementations beyond linear response are scarcer still, with our report of relativistic QR-EOMCC<sup>115</sup> being, to the best of our knowledge, the first to appear in the literature. This implementation allowed us to gauge the performance of more approximate approaches such as TDDFT and TDHF in the calculation of hyperpolarizabilities, two-photon absorption cross-sections and Verdet constants. However, as discussed above QR-CC and QR-EOMCC are not equivalent, and it is desirable to further characterize the behavior of the latter with respect to the former across the periodic table, before carrying out more extensive applications with the more approximate QR-EOMCC scheme.

The aim of the current work is therefore to report our implementation of quadratic response coupled cluster for relativistic Hamiltonians, capable of handling for both static and frequency-dependent perturbations involving electric or magnetic operators. We showcase it by providing a first comparison of how QR-CC and QR-EOMCC behave as one goes towards the bottom of the periodic table. We thereby chose to re-investigate the dipole first hyperpolarizabilities of hydrogen halides, and the Verdet constants of heavy noble gas atoms as they show significant relativistic effects.<sup>115</sup> Going further than this previous work, we carried out a more extensive exploration on the effect of the Hamiltonian on these properties, and investigated the properties of systems made up of superheavy elements, such as the Tennessine hydride molecule and the Oganesson atom.

Tennessine and Oganesson, whose existence has been recognized by IUPAC and IUPAC in 2015, are the two heaviest elements known. They have been synthesized at the Joint Institute for Nuclear Research in Dubna by nuclear fusion upon bombardment of Berkelium and Californium targets by between atoms of Calcium-48 ions, respectively.<sup>116,117</sup> While they

are expected to be members of groups 17 and 18, the difficulties in their production–only a few atoms are generated at a time, and their lifetimes are in the order of milliseconds–present formidable challenges to the experimental characterization of their physico-chemical properties,<sup>118</sup> making theoretical work an indispensable tool to learn about their electronic structure.<sup>69</sup> In view of their large polarizabilities and more pronounced spin-orbit coupling than that in 6p, 5d and 5f block elements, they are also of potential interest as probes for any subtle difference between CC and EOMCC in the calculation of response properties.

## Theory and Implementation

### Quadratic Response Theory

As was the case in our previous work on coupled cluster linear response<sup>113</sup> (LR-CC) and EOM-CC quadratic response<sup>115</sup> (QR-EOMCC), our work is carried out within the framework of the quasienergy formulation of response theory.<sup>31</sup> For the sake of brevity, we only review the formalism for CC quadratic response (QR-CC), and refer to the supplementary information for the working equations of QR-EOMCC as presented in.<sup>115</sup> Throughout the text, the CC acronym will imply the use of coupled cluster singles and doubles (CCSD) wavefunctions.

We shall remain within the no-pair approximation,<sup>83,119,120</sup> with the electronic part of the unperturbed molecular Hamiltonian given by

$$\hat{H}_0 = \sum_{pq} h_q^p \{ \hat{a}_p^\dagger \hat{a}_q \} + \frac{1}{4} \sum_{pqrs} V_{rs}^{pq} \{ \hat{a}_p^\dagger \hat{a}_q^\dagger \hat{a}_s \hat{a}_r \} \quad (1)$$

where and  $p, q, r, s$  denote general (occupied or positive energy virtual) indexes,  $h_{pq} = \langle p | \hat{h} | q \rangle$  denotes matrix elements of the one-body operator  $\hat{h}$ , and  $V_{rs}^{pq} = \langle pq | \hat{g} | rs \rangle - \langle pq | \hat{g} | sr \rangle$  the anti-symmetrized matrix elements of the two-body operator  $\hat{g}$ . In the calculations reported in this work,  $\hat{g}$  corresponds to Coulomb operator. In our current implementation, Gaunt or

Breit interactions are assumed to be treated in an effective manner.<sup>121–124</sup> External time-(in)dependent perturbations will be represented by one-body operators

$$\hat{Y} = \sum_{pq} Y_q^p \{ \hat{a}_p^\dagger \hat{a}_q \} \quad (2)$$

where  $Y_q^p = \langle p | \hat{Y} | q \rangle$ .

Due to the fact that in CC response theory the time-dependent quasienergy Lagrangian<sup>31</sup> is made stationary with respect to the wavefunction parametrization (CC amplitudes and multipliers), we can use the  $(2n + 1)$  and  $(2n + 2)$  rules in perturbation theory.<sup>13,31</sup> The calculation of a third-order property such as quadratic response, thus only requires the determination of the unperturbed and first-order perturbed CC amplitudes and Lagrange multipliers.

The unperturbed CC amplitudes  $T$  and Lagrange multipliers  $\bar{T}$  are defined as

$$T = T_1 + T_2 = \sum_{ai} t_i^a \{ \hat{a}_a^\dagger \hat{a}_i \} + \frac{1}{4} \sum_{abij} t_{ij}^{ab} \{ \hat{a}_a^\dagger \hat{a}_b^\dagger \hat{a}_j \hat{a}_i \} = \sum_{ai} t_i^a \hat{\tau}_1 + \frac{1}{4} \sum_{abij} t_{ij}^{ab} \hat{\tau}_2 \quad (3)$$

$$\bar{T} = \bar{T}_1 + \bar{T}_2 = \sum_{ia} \bar{t}_a^i \{ \hat{a}_i^\dagger \hat{a}_a \} + \frac{1}{4} \sum_{ijab} \bar{t}_{ab}^{ij} \{ \hat{a}_i^\dagger \hat{a}_j^\dagger \hat{a}_b \hat{a}_a \} = \sum_{ia} \bar{t}_a^i \hat{\tau}_1^\dagger + \frac{1}{4} \sum_{ijab} \bar{t}_{ab}^{ij} \hat{\tau}_2^\dagger \quad (4)$$

with  $a, b$  for particle lines and  $i, j$  for hole lines. As a shorthand notation, in the following we shall use greek letters  $\{ \mu, \nu, \sigma \}$  to represent the strings of second quantization operators, with subscripts to represent single or double excitation; for instance,  $\hat{\tau}_{\mu_1} \equiv \hat{\tau}_1 = \hat{a}_a^\dagger \hat{a}_i$  whereas  $\hat{\tau}_\mu$  will represent a generic (either single or double) excitation operator. Conversely,  $\hat{\tau}_\mu^\dagger$  will denote a de-excitation operator, which is biorthogonal to operator  $\hat{\tau}_\mu$ , that is,  $\langle R | \hat{\tau}_\mu^\dagger \hat{\tau}_\nu | R \rangle = \delta_{\mu\nu}$ , with  $|R\rangle$  representing the reference state, here a single Slater determinant made up of molecular orbitals—or molecular spinors whenever the Hamiltonian accounts for spin-orbit coupling. Also,  $|\mu\rangle$  denotes the ensemble of excited determinants with respect to the reference.

From the exponential ansatz for the CC wavefunction<sup>125,126</sup>

$$|\text{CC}\rangle = \exp(T)|\text{R}\rangle, \quad (5)$$

the time-independent Dirac (Schrödinger) wave equation

$$\hat{H}_0|\text{CC}\rangle = E|\text{CC}\rangle \quad (6)$$

and the  $\Lambda$  operator

$$\langle\Lambda| = \langle\text{R}| + \sum_{\mu} \bar{t}_{\mu} \langle\mu| \exp(-T), \quad (7)$$

we have the unperturbed amplitudes and multipliers obtained from the equations

$$\langle\mu| \bar{\mathbf{H}} |\text{R}\rangle = 0 \quad (8)$$

$$\bar{t} \bar{\mathbf{H}} + \eta = 0 \quad (9)$$

where  $\bar{\mathbf{H}}$  is matrix representation of the normal-ordered similarity transformed Hamiltonian. The definitions of  $\bar{\mathbf{H}}$  and  $\eta$  are given in table 1. Further details on the evaluation of these equations in our implementation can be found in.<sup>84</sup>

After solving for the unperturbed wave function parameters, the first-order parameters are next obtained by solving the response equations<sup>31,113,115</sup>

$$(\bar{\mathbf{H}} - \omega_Y \mathbf{I}) \overset{Y}{t}(\omega_Y) + \xi^Y = 0 \quad (10a)$$

$$\overset{Y}{t}(\omega_Y) (\bar{\mathbf{H}} + \omega_Y \mathbf{I}) + \eta^Y + \mathbf{F} \overset{Y}{t}(\omega_Y) = 0, \quad (10b)$$

where  $\mathbf{I}$  is the identity matrix. We employ the shorthand notation  $\overset{Y}{t}, \overset{Y}{\bar{t}}$  to describe the first-order perturbed amplitudes and multipliers, obtained for perturbation  $\hat{Y}$  at frequency  $\omega_Y$ , respectively. We note that, in contrast to the first-order response equations in QR-EOMCC, the equations for the first-order perturbed multipliers depend on the first-order perturbed

amplitudes. The definitions of terms  $\mathbf{F}$ ,  $\xi^Y$ ,  $\eta^Y$  are also given in table 1.

The frequency-(in)dependent quadratic response function is given by the expression

$$\begin{aligned} \langle\langle Z; X, Y \rangle\rangle_{\omega_X, \omega_Y} &= \frac{1}{2} C^{\pm\omega} P(X(\omega_X), Y(\omega_Y), Z(\omega_Z)) \\ &\times \left\{ \left[ \frac{1}{2} \mathbf{F}^X + \frac{1}{6} \mathbf{G}^{\bar{x}} t(\omega_X) \right]^Y t(\omega_Y) + \frac{\bar{x}}{t(\omega_X)} \left[ \mathbf{A}^Y + \frac{1}{2} \mathbf{B}^Y t(\omega_Y) \right]^Z t(\omega_Z) \right\} \end{aligned} \quad (11)$$

where the perturbing frequencies satisfy the relationship  $\omega_Z = -(\omega_X + \omega_Y)$ . The operator  $P(X(\omega_X), Y(\omega_Y), Z(\omega_Z))$  takes care of the permutation of the perturbing operators, and

$$C^{\pm\omega} f^{XYZ}(\omega_X, \omega_Y, \omega_Z) = f^{XYZ}(\omega_X, \omega_Y, \omega_Z) + [f^{XYZ}(-\omega_X, -\omega_Y, -\omega_Z)]^* \quad (12)$$

is used for the symmetrization of the response functions,<sup>31</sup> which requires the solution of response  $f^{XYZ}(\omega_X, \omega_Y, \omega_Z)$  also for the negative of the frequencies (inverting the frequencies followed by complex conjugation). Eq. 11 can also be rewritten as

$$\langle\langle X, Y, Z \rangle\rangle_{\omega_Y, \omega_Z} = \frac{1}{2} C^{\pm\omega} P(X(\omega_X), Y(\omega_Y), Z(\omega_Z)) \times \left\{ [O^{X,Y}] + [O^{\bar{X},Y}] \right\}^Z t(\omega_Z), \quad (13)$$

where  $O^{X,Y}$  and  $O^{\bar{X},Y}$  group the terms involving contractions only with perturbed amplitudes or with both perturbed amplitudes and multipliers, respectively:

$$O^{X,Y} = \left[ \frac{1}{2} \mathbf{F}^X + \frac{1}{6} \mathbf{G}^{\bar{x}} t(\omega_X) \right]^Y t(\omega_Y) = \frac{1}{2} \mathbf{F}^{X,Y} t(\omega_Y) + \frac{1}{6} \mathbf{G}^{\bar{x}} t(\omega_X)^Y t(\omega_Y) \quad (14a)$$

$$O^{\bar{X},Y} = \frac{\bar{x}}{t(\omega_X)} \left[ \mathbf{A}^Y + \frac{1}{2} \mathbf{B}^Y t(\omega_Y) \right] = \frac{\bar{x}}{t(\omega_X)} \mathbf{A}^Y + \frac{1}{2} \frac{\bar{x}}{t(\omega_X)} \mathbf{B}^Y t(\omega_Y) \quad (14b)$$

and that for all combinations allowed by the  $C^{\pm\omega} P$  product.

As is the case for  $\bar{\mathbf{H}}$  and  $\mathbf{F}$ ,<sup>113,115</sup> the  $\mathbf{F}^{\mathbf{X}}$ ,  $\mathbf{A}^{\mathbf{Y}}$ ,  $\mathbf{G}$  and  $\mathbf{B}$  tensors, given by the expression in the table 1, are never constructed explicitly but rather as contractions with the perturbed amplitudes and/or multipliers. The programmable expressions required to assemble the  $\mathbf{G}^{XYZ} t t t$  term are presented in the supplementary information. The programmable expressions

Table 1: Expressions for the tensors appearing in the coupled cluster quadratic response functions as well as in the linear response equations determining perturbed amplitudes and Lagrange multipliers. Here  $|\mathbf{R}\rangle$  denotes the reference state in the definition of the coupled cluster wave function  $|\mathbf{CC}\rangle = \exp(T)|\mathbf{R}\rangle$  and for the  $\langle\Lambda| = \langle\mathbf{R}| + \sum_{\mu} \hat{t}_{\mu} \langle\bar{\mu}|$  operator, with  $\langle\bar{\mu}| = \langle\mathbf{R}|\hat{\tau}_{\mu}^{\dagger} \exp(-T)$ . Finally,  $\hat{X}$  and  $\hat{Y}$  denote one-body perturbation operators. We note that  $\bar{\mathbf{H}}$  is strictly equivalent to the  $\mathbf{A}$ , the CC Jacobian defined by Christiansen et al.<sup>31</sup>.

$\eta_{\nu}$	$\langle\mathbf{R} [\hat{H}_0, \hat{\tau}_{\mu}] \mathbf{CC}\rangle$
$\bar{\mathbf{H}}_{\mu\nu}$	$\langle\bar{\mu} [\hat{H}_0, \hat{\tau}_{\mu}] \mathbf{CC}\rangle$
$\mathbf{F}_{\mu\nu}$	$\langle\Lambda [[\hat{H}_0, \hat{\tau}_{\mu}], \hat{\tau}_{\nu}] \mathbf{CC}\rangle$
$\boldsymbol{\eta}_{\mu}^Y$	$\langle\Lambda [\hat{Y}, \hat{\tau}_{\mu}] \mathbf{CC}\rangle$
$\boldsymbol{\xi}_{\mu}^Y$	$\langle\bar{\mu} \hat{Y} \mathbf{CC}\rangle$
$\mathbf{F}_{\mu\nu}^X$	$\langle\Lambda [[\hat{X}, \tau_{\mu}], \tau_{\nu}] \mathbf{CC}\rangle$
$\mathbf{G}_{\mu\nu\sigma}$	$\langle\Lambda [[[\hat{H}_0, \tau_{\mu}], \tau_{\nu}], \tau_{\sigma}] \mathbf{CC}\rangle$
$\mathbf{A}_{\mu\nu}^Y$	$\langle\bar{\mu} [\hat{Y}, \tau_{\nu}] \mathbf{CC}\rangle$
$\mathbf{B}_{\mu\nu\sigma}$	$\langle\bar{\mu} [[\hat{H}_0, \tau_{\nu}], \tau_{\sigma}] \mathbf{CC}\rangle$

for  $\mathbf{F}^X$ ,  $\mathbf{A}^Y$  and  $\mathbf{B}$  can be obtained from minor modifications of those already presented in our previous work.<sup>113,115</sup>

## Implementation details

Our QR-CC implementation has been carried out in the ExaCorr module<sup>84</sup> of the relativistic quantum chemistry program DIRAC.<sup>127</sup> Below we provide details on the implementation of the QR-CC response function calculation, and refer the reader to prior works concerning (a) the solution of ground-state amplitudes and multipliers;<sup>84</sup> and (b) the solution of first-order response equations,<sup>113</sup> which leveraged our prior implementation of a generalized Davidson eigenvalue solver<sup>102,128</sup> to implement the solution of systems of linear equations.<sup>129</sup> We recall that through the use of the TAL-SH tensor library,<sup>130</sup> a modular component of the ExaTENSOR library,<sup>131</sup> all tensor operations in our code are parallelized via OpenMP and can be offloaded to NVIDIA or AMD GPUs whenever these are available.

In our implementation, we divide the calculation into different levels of subroutines: (a) a top-level driver to organize calculations for  $\omega$  and  $-\omega$  and to apply the symmetrization operator as in Eq. 12; (b) a driver that calculates  $\xi^Y, \eta^Y$  for all operators under consideration,

solves all corresponding linear response equations for either QR-CC and QR-EOMCC, and calls the driver to calculate the appropriate response function.

In the case of QR-CC, the response function driver carries out the six permutations between the triplet of  $X, Y, Z$  operators; it calls a subroutine that calculates the terms within the curly braces in Eq.13 for a given pair of operators  $X, Y$  and stores it on set of 2-/4-dimension tensors (singles and doubles manifolds) and performs the contraction with the  $\overset{z}{t}$  perturbed amplitudes. This allows us to, if desired, extract the contributions from each of the four terms (for each triplet of operators) and further break these down in terms of the contributions from the singles and doubles manifolds.

## Computational details

All QR-CC, QR-EOMCC calculations were carried out with a development version (revision number 8ef365b7) of the DIRAC code.<sup>127,132</sup> All coupled cluster calculations have been carried out in GPU-accelerated nodes.

As done in our prior EOM-QR calculations,<sup>115</sup> we have used some of the functionality connected to the Cholesky-decomposition approach in ExaCorr<sup>84</sup> to avoid the explicit construction of the 2-electron repulsion integral tensor in AO basis in the integral transformation step and with that reduce the memory footprint of our calculations. We employed a thresholds of  $10^{-5}$  for all systems except HAt and HTs, for which the threshold was set to  $10^{-4}$ . The outcome of response calculations is not significantly affected by these approximations.

The Dunning basis set<sup>133-135</sup> augmented by three diffuse functions (denoted by t-aug-cc-pVTZ) was used for the hydrogen atom. For all other atoms, the Dyall triple zeta sets (denoted by t-aug-dyall.v3z) were employed in general, though in some cases and for elements up to bromide the t-aug-cc-pVTZ set was used to make a direct comparison to our prior EOM-QR calculations<sup>115</sup> possible. The diffuse functions in question were automatically generated by DIRAC as an even-tempered sequence based on the most diffuse exponents for

all angular momenta primitives in the original basis.

In addition to the non-relativistic<sup>136,137</sup>(as activated by the `.Levy-Leblond` keyword) and eXact 2-Component (X2C) relativistic,<sup>123</sup> in the coupled cluster calculations we also investigated the molecular mean-field X2C method based on the Dirac-Coulomb ( ${}^2\text{DC}^M$ ) and Dirac-Coulomb-Gaunt ( ${}^2\text{DCG}^M$ ) Hamiltonians, as well as the spin-free (SF) variants of the X2C and  ${}^2\text{DCG}^M$  Hamiltonians. In what follows, we shall use the term orbital as shorthand for both spinors and spin-orbitals, depending on the Hamiltonian used in the calculation. In X2C calculations including spin-orbit coupling, we make use of atomic-mean field SOC integrals, obtained from a calculation employing the Douglas-Kroll-Hess Hamiltonian.

The relativistic and non-relativistic calculations have been carried out with the Gaussian type<sup>138</sup> and point charge nucleus model, respectively.

The molecular structures employed in our calculations have been taken from Huber and Herzberg<sup>139</sup> for HX (X=F, Cl, Br, I), from Gomes and Visscher<sup>140</sup> for HAt, and from de Farias<sup>141</sup> for HTs, so respectively: H-F (0.91680 Å), H-Cl (1.27455 Å), H-Br (1.41443 Å), H-I (1.60916 Å), H-At (1.722 Å) and H-Ts (1.9676 Å). As the choice of orientation in these systems may affect the signs of the electric dipole and first hyperpolarizability (but not their absolute value), we note our results have been tabulated following the convention that the heavy atoms are placed at the origin of the coordinate system, with the molecular axis aligned with the z axis of the coordinate system.

For the most part we retained the correlation spaces defined by Yuan et al.<sup>115</sup>, which include valence electrons and virtual orbitals with energies up to 5 a.u.; However, in some cases (Xe, Rn, Og) we also explored the correlation of the  $(n - 1)d$  shell and in selected cases, larger virtual cutoffs (100 a.u.), and in others (HF, HCl, HBr) we also carried out calculations correlating all electrons and all virtual orbitals.

EOM-CC excitation energy calculations exploiting point-group symmetry were carried out for the noble gas atoms using the RELCCSD module of DIRAC with the  ${}^2\text{DC}^M$  and the same basis sets and correlating spaces as employed for the QR-CC calculations.

All inputs, outputs and structures used in this paper are available in the zenodo repository as supplemental information.

## Results and discussion

In the sections below we discuss our results for the first hyperpolarizability and Verdet constant for systems across the periodic table. We note that the choice of computational setup concerning the basis sets and correlation space, as well as a comparison to the B3LYP functional, have been discussed in detail in our work discussing the implementation of QR-EOMCC.<sup>115</sup> Therefore, in the following we will mostly focus on a comparison between QR-CC and QR-EOMCC for different Hamiltonians.

### First hyperpolarizability of hydrogen halides (HX, X=F–Ts)

Due to the symmetry of the systems under consideration, we restrict ourselves to the calculation of the parallel component of the static first hyperpolarizability ( $\beta_{||}$ )<sup>142</sup>

$$\beta_{||} = \frac{1}{5} \sum_{i=x,y,z} (\beta_{iiz} + \beta_{izi} + \beta_{zii}) \quad (15)$$

where the  $\beta_{ijk}$  element is given by the sum-over-states expression:<sup>1</sup>

$$\beta_{ijk}(-\omega_\sigma; \omega_1, \omega_2) = \sum P_{-\sigma,1,2} \sum_{n,m} \frac{\langle 0 | \hat{\mu}_i | n \rangle \langle n | \hat{\mu}_j | m \rangle \langle m | \hat{\mu}_k | 0 \rangle}{(\omega_{n0} - \omega_\sigma)(\omega_{m0} - \omega_2)} \quad (16)$$

with  $\hat{\mu}_i$  the Cartesian components of the electric dipole operators,  $\sum P_{-\sigma,1,2}$  indicating the sum of six terms by permuting the pairs  $(i, -\omega_\sigma)$ ,  $(j, \omega_1)$ ,  $(k, \omega_2)$ , and  $\omega_{n0}$  denoting the excitation energy between the ground state and excited state  $n$ . In the following we only

calculated two unique components,  $\beta_{zzz}$  and  $\beta_{zxx}$ , so that  $\beta_{||}$  and  $\beta_{\text{aniso}}$  are calculated from

$$\beta_{||} = \frac{3}{5}(\beta_{zzz} + 2\beta_{zxx}) \quad (17)$$

$$\beta_{\text{aniso}} = \beta_{zzz} - 3\beta_{zxx} \quad (18)$$

respectively. Our results for the frequency-independent case are summarized in tables 2 and 3 for the  $\beta_{||}$  and  $\beta_{\text{aniso}}$ . To illustrate the trends for the individual components, in figure 1 we present results for the SF- $^2\text{DC}^M$  and  $^2\text{DC}^M$  Hamiltonians, while in tables 1 and 2 in the SI we report the values for the  $\beta_{zzz}$  and  $\beta_{zxx}$  components respectively for all Hamiltonians under consideration.

We recall that our use of a Gaussian nuclear model and Dyal bases in all calculations makes for a slightly different setup than that of Yuan et al.<sup>115</sup>. For ease of comparison, we also provide results obtained with the Dunning basis set on the halogens, and note small discrepancies for calculations with the Levy-Leblond Hamiltonian arising from the difference in nuclear model.

Focusing first on the QR-EOMCC and QR-CC results for the different Hamiltonians for both  $\beta_{||}$  and  $\beta_{\text{aniso}}$ , we observe that for HF and HCl scalar relativistic effects are dominant, with spin-orbit effects representing less than 1% of the total response, something to be expected for these molecules which contain only light elements. For HBr we see that spin-orbit coupling is of some importance—in absolute terms, the hyperpolarizabilities increase with respect to spin-free calculations by about 5% (20%) for  $\beta_{||}$  QR-CC (QR-EOMCC) and reach about 8% for HI and 10 % for HAt. For HTs, on the other hand, spin-orbit coupling is the dominant effect, with nearly a twofold increase in value compared to spin-free calculations. For HF to HI the absolute values for  $\beta_{\text{aniso}}$  are typically rather small, and become larger for HAt and HTs.

Table 2: QR-CCSD (CC) and QR-EOMCCSD (EOM) values for the  $\beta_{||}$  component (in a.u.) of the static first hyperpolarizability of hydrogen halides, as well as their difference ( $\Delta\beta_{||}$ ). All calculations correlate eight (valence) electrons virtuals up to 5 a.u., except those marked by “\*”, in which all electrons and virtuals are correlated; †calculated with Dunning basis sets for the halogens; nc: not calculated.

Method	Hamiltonian	HF	HCl	HBr	HI	HAt	HTs
CC	LL	-8.0441	-8.2236	-5.5096	1.5590	9.9337	46.4544
	LL†	-8.0370	-8.7902	-5.8960	nc	nc	nc
	SF-X2C	-8.0483	-8.0824	-4.1250	6.3168	35.6445	173.6980
	SF- <sup>2</sup> DC <sup>M</sup>	-8.0483	-8.0821	-4.1253	6.3164	35.6457	173.9446
	X2C	-8.0537	-8.1031	-4.3473	5.7901	39.5212	476.3573
	X2C†	-8.0407	-8.6627	-4.7106	nc	nc	nc
	<sup>2</sup> DC <sup>M</sup>	-8.0498	-8.0942	-4.3343	5.7341	39.7956	495.1556
	<sup>2</sup> DC <sup>M,*</sup>	-7.9142	-8.0537	-4.7243	nc	nc	nc
	<sup>2</sup> DCG <sup>M</sup>	-8.0494	-8.0918	-4.3212	5.7574	39.8091	493.6418
	EOM	LL	-7.4972	-5.6034	-0.2535	11.1413	23.5288
LL†		-7.5315	-6.2493	-0.6946	nc	nc	nc
SF-X2C		-7.4993	-5.4499	1.1741	15.6862	46.4367	164.0866
SF- <sup>2</sup> DC <sup>M</sup>		-7.4994	-5.4502	1.1731	15.6839	46.4288	164.1359
X2C		-7.5046	-5.4712	0.9285	14.8533	45.5480	405.8769
X2C†		-7.5333	-6.1101	0.5181	nc	nc	nc
<sup>2</sup> DC <sup>M</sup>		-7.5009	-5.4627	0.9445	14.8124	45.8277	423.0797
<sup>2</sup> DC <sup>M,*</sup>		-7.6050	-5.6405	-0.4133	nc	nc	nc
<sup>2</sup> DCG <sup>M</sup>		-7.5016	-5.4658	0.9341	14.7813	45.8455	422.7453
$\Delta\beta_{  }$		LL	-0.5469	-2.6203	-5.2561	-9.5822	-13.5951
	LL†	-0.5055	-2.5409	-5.2014	nc	nc	nc
	SF-X2C	-0.5490	-2.6324	-5.2991	-9.3694	-10.7921	9.6114
	SF- <sup>2</sup> DC <sup>M</sup>	-0.5490	-2.6319	-5.2985	-9.3675	-10.7831	9.8088
	X2C	-0.5491	-2.6319	-5.2758	-9.0631	-6.0268	70.4803
	X2C†	-0.5074	-2.5526	-5.2287	nc	nc	nc
	<sup>2</sup> DC <sup>M</sup>	-0.5490	-2.6316	-5.2787	-9.0782	-6.0321	72.0758
	<sup>2</sup> DC <sup>M,*</sup>	-0.3092	-2.4132	-4.3110	nc	nc	nc
	<sup>2</sup> DCG <sup>M</sup>	-0.5478	-2.6261	-5.2553	-9.0239	-6.0364	70.8965

In all cases, there are no significant differences between the (SF-)X2C and (SF-)<sup>2</sup>DC<sup>M</sup> Hamiltonians, in spite of the more approximate starting point of the X2C calculations, and the effect of the Gaunt interaction is only non-negligible for the HAt and HTs molecules (though it only contributes to about 1%).

We have noticed small differences between our results and those previously reported,<sup>115</sup>

the latter showing larger (in absolute value) hyperpolarizabilities. We have traced this difference to the use of Dyall basis sets for the current calculations, as opposed to the Dunning basis sets. This difference can be understood as a consequence of the bias towards somewhat less diffuse exponents as part of the process of obtaining relativistic energy-optimized basis sets.

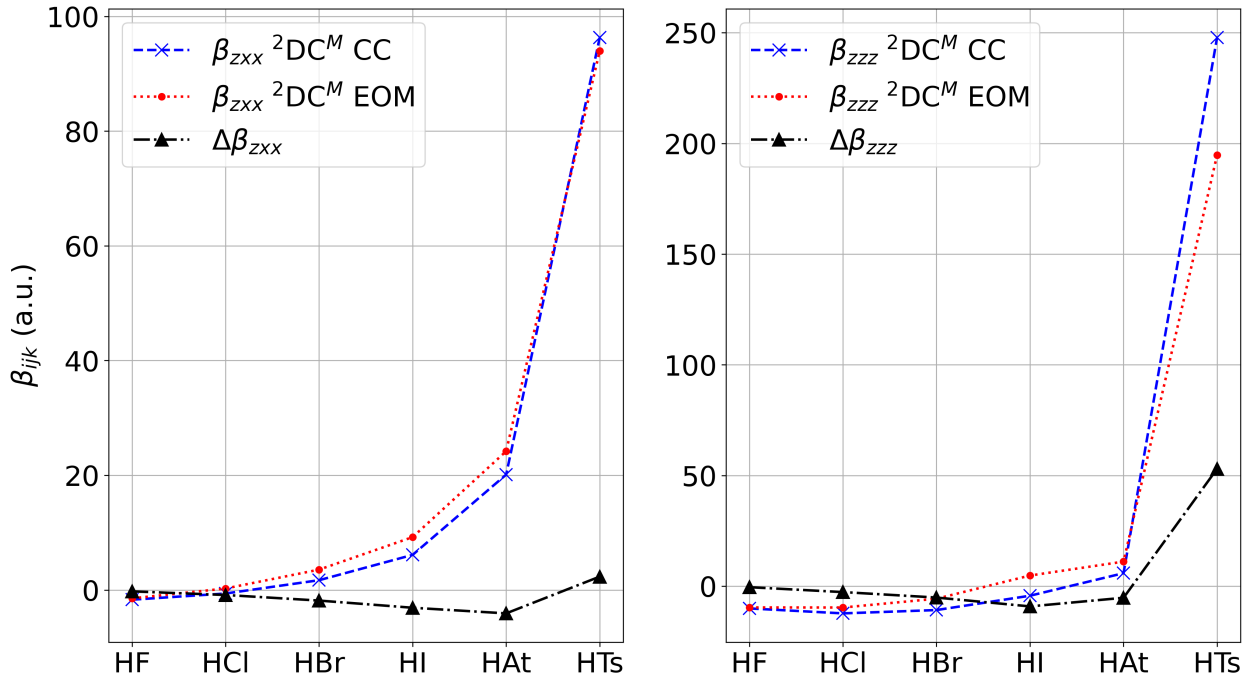


Figure 1: QR-CC and QR-EOMCC dipole hyperpolarizabilities components ( $\beta_{zxx}$  and  $\beta_{zzz}$ , in a.u.) and the respective differences ( $\Delta\beta_{zxx}$  and  $\Delta\beta_{zzz}$ , in a.u.) calculated with the  ${}^2\text{DC}^M$  Hamiltonians for the HX series, upon correlating the  $nsnp$  shells (and with virtual threshold at 5 a.u.).

Focusing now first on QR-CC values for  $\beta_{||}$ , for HF to HBr we observe negative values (similar in magnitude for HF and HCl, but less negative for HBr), and positive for HI, HAt, and HTs, with rather large values for the latter molecule. These trends result from the fact that the clearly negative  $\beta_{zzz}$  component for HF initially becomes less negative as the halogen becomes heavier, changes sign for HAt, and becomes strongly positive for HTs. The  $\beta_{zxx}$  component shows a similar trend, with positive values from HBr onwards, but is smaller in magnitude than  $\beta_{zzz}$  for most systems. These trends are qualitatively the same for QR-EOMCC across the series, with as important difference that the sign change in  $\beta_{||}$

upon going down the series already occurs for HBr.

Quantifying the differences between QR-CC and QR-EOMCC by computing  $(\Delta\beta_{||})$ , we see that differences are small for HF but become non-negligible already for HCl and remain sizable for the other species. In relative terms, the differences for  $\beta_{||}$  are about 6% for HF, but grow to about 30% for HCl, 120 % for HBr and 150% for HI. For the very large positive hyperpolarizability of HTs, the difference is in absolute sense the largest, but amounts to only 15% of the  ${}^2\text{DCG}^M$  value. For the more accessible HAt molecule, the effect is similar but less pronounced. Finally, we see essentially the same trends when correlating more electrons and virtuals in the lighter systems (HF to HBr), though we do observe a somewhat smaller difference between QR-CC and QR-EOMCC for HBr than when only the valence is correlated. This is driven by a larger increase in the  $\beta_{zzz}$  for QR-EOMCC than for QR-CC.

We note the situation is a bit different for  $\beta_{\text{aniso}}$ , where we observe that apart from HTs, the difference between QR-CC and QR-EOMCC is fairly modest across the series.

Going beyond the static case, in figure 2 we present the results for second harmonic generation (SHG) calculations on HI, which corresponds to the case in which  $\omega_B = \omega_C = \omega_A/2$ . As this property has been discussed in detail in our work presenting QR-EOMCC,<sup>115</sup> we refer the reader to it for further details on the behavior of the dispersion curves. We nevertheless highlight the fact that that in the region around  $\omega = \omega_B = \omega_C = 0.1$  a.u., corresponding to half the excitation energy of the spin-orbit allowed transition towards the  $a^3\Pi_{0+}$  state, we see the expected pole for the quadratic response functions. Beside that, we observe that across the range of frequencies sampled, the difference between QR-CC and QR-EOMCC results amounts to a constant shift.

Table 3: QR-CCSD (CC) and QR-EOMCCSD (EOM) values for the  $\beta_{\text{aniso}}$  component (in a.u.) of the static first hyperpolarizability of hydrogen halides, as well as their difference ( $\Delta\beta_{\text{aniso}}$ ). All calculations correlate eight (valence) electrons virtuals up to 5 a.u., except those marked by “\*”, in which all electrons and virtuals are correlated; †calculated with Dunning basis sets for the halogens; nc: not calculated.

Method	Hamiltonian	HF	HCl	HBr	HI	HAt	HTs
CC	LL	-4.9459	-10.3349	-14.5008	-16.3776	-18.5536	-50.1339
	LL†	-4.6309	-10.0969	-14.3693	nc	nc	nc
	SF-X2C	-4.9455	-10.4108	-15.4252	-20.1042	-41.2161	-191.5107
	SF- <sup>2</sup> DC <sup>M</sup>	-4.9454	-10.4091	-15.4184	-20.0927	-41.1858	-191.6326
	X2C	-4.9536	-10.4424	-16.0964	-24.8101	-83.2791	-599.5770
	X2C†	-4.6278	-10.1948	-15.9223	nc	nc	nc
	<sup>2</sup> DC <sup>M</sup>	-4.9467	-10.4348	-16.0811	-25.0659	-84.7735	-618.4277
	<sup>2</sup> DC <sup>M,*</sup>	-5.1300	-10.6165	-16.5149	nc	nc	nc
	<sup>2</sup> DCC <sup>M</sup>	-4.9478	-10.4450	-16.1219	-25.1406	-84.9810	-617.7646
	EOM	LL	-5.2227	-10.2724	-14.6625	-15.0853	-16.4412
LL†		-4.9146	-9.9864	-14.4596	nc	nc	nc
SF-X2C		-5.2236	-10.3699	-15.8135	-19.9561	-43.5784	-195.9931
SF- <sup>2</sup> DC <sup>M</sup>		-5.2234	-10.3687	-15.8100	-19.9571	-43.5978	-196.3284
X2C		-5.2315	-10.4017	-16.4911	-24.6949	-85.2353	-553.0503
X2C†		-4.9126	-10.1052	-16.2428	nc	nc	nc
<sup>2</sup> DC <sup>M</sup>		-5.2248	-10.3948	-16.4807	-24.9707	-86.8113	-570.8098
<sup>2</sup> DC <sup>M,*</sup>		-5.3591	-10.5605	-16.7843	nc	nc	nc
<sup>2</sup> DCC <sup>M</sup>		-5.2252	-10.4008	-16.5012	-24.9851	-86.8673	-570.0000
$\Delta\beta_{\text{aniso}}$		LL	0.2768	-0.0624	0.1618	-1.2923	-2.1124
	LL†	0.2838	-0.1105	0.0903	nc	nc	nc
	SF-X2C	0.2780	-0.0409	0.3883	-0.1482	2.3622	4.4824
	SF- <sup>2</sup> DC <sup>M</sup>	0.2781	-0.0404	0.3915	-0.1357	2.4120	4.6959
	X2C	0.2780	-0.0407	0.3947	-0.1151	1.9562	-46.5267
	X2C†	0.2848	-0.0896	0.3205	nc	nc	nc
	<sup>2</sup> DC <sup>M</sup>	0.2781	-0.0400	0.3997	-0.0952	2.0379	-47.6178
	<sup>2</sup> DC <sup>M,*</sup>	0.2291	-0.0560	0.2695	nc	nc	nc
	<sup>2</sup> DCC <sup>M</sup>	0.2774	-0.0442	0.3793	-0.1555	1.8864	-47.7646

In the following we look more closely at the differences between QR-CC and QR-EOMCC by analyzing the contributions from the different terms to the response functions, found in tables 4 and 3 for QR-CC and QR-EOMCC respectively, as we go across the series from HF to HI.

For this analysis, it is interesting to also consider the results for the static dipole po-

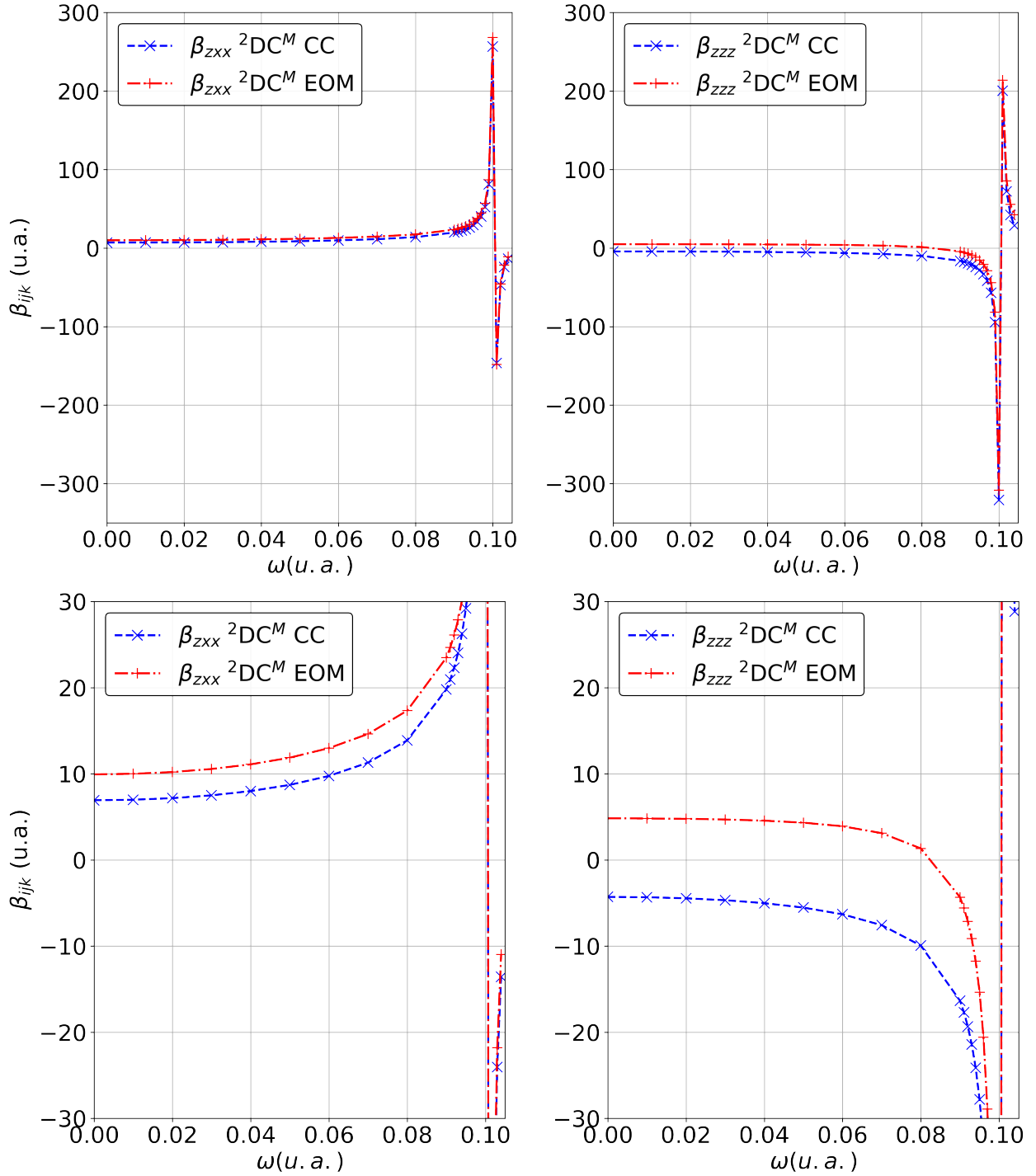


Figure 2: QR-CC and QR-EOMCC  ${}^2\text{DC}^M$  dispersion curves for the  $\beta_{zzz}, \beta_{zxx}$  components (top: general view; bottom: detailed view of the low-frequency region) of the hyperpolarizability of the HI molecule for second harmonic generation (SHG) calculations ( $\omega = \omega_B = \omega_C$ , in a.u.). We note the pole at around 0.10 a.u. corresponding to half of the excitation energy towards the  $\alpha^3\Pi_{0+}$  state.<sup>115</sup>

larizabilities for the same molecules, since the difference between LR-CC and LR-EOMCC calculations is connected to the presence of the  $\mathbf{F}t^Y$  term in the LR-CC response function (and therefore the right-hand side transition moment), whereas LR-EOMCC employs a simpler expression (for both methods perturbed amplitudes  $t^Y$  are obtained from eq. 10a).

These dipole polarizabilities, shown in figure 3 (values for dipole moments and polarizabilities are reported in the SI) increase across the series, which is consistent with the increase in size of the halides accompanied by their decreasing electronegativity. The differences between CC and EOMCC do increase across the series for the  $\alpha_{zz}$  and  $\alpha_{xx}$  components and consequently, for the mean polarizability  $\bar{\alpha}$  as well. However, in contrast to the hyperpolarizabilities, in relative terms these differences are roughly the same and of about 2% for  $\alpha_{zz}$  and 1.5% for  $\alpha_{xx}$ .

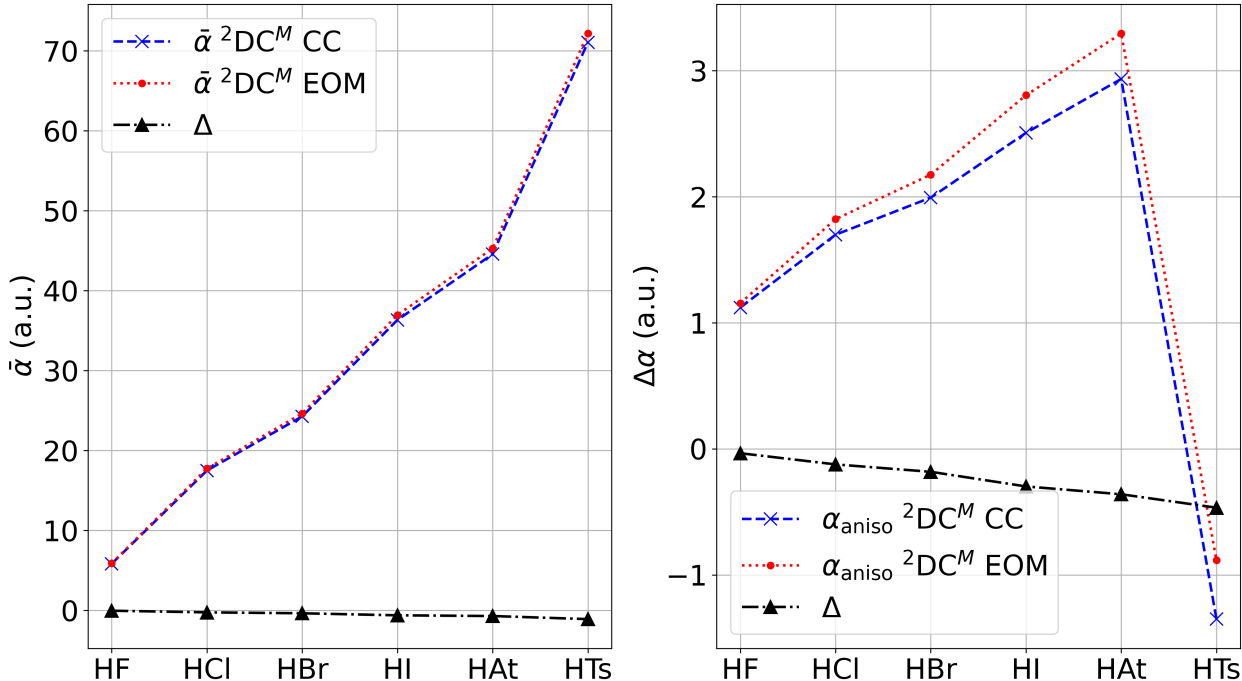


Figure 3: Mean dipole polarizabilities (left,  $\bar{\alpha} = 1/3(\alpha_{zz} + 2\alpha_{xx})$  in a.u.) and anisotropies (right,  $\Delta\alpha = \alpha_{zz} - \alpha_{xx}$  in a.u.) calculated with  ${}^2\text{DC}^M$  Hamiltonian for the HX series with LR-CC and LR-EOMCC, upon correlating the  $nsnp$  shells (and with virtual threshold at 5 a.u.). The absolute differences between the two approaches ( $\Delta$ , in a.u.) are also presented.

The difference between CC and EOMCC is more strongly felt for the anisotropy, which

is about 3% for HF, but 8-12% for HCl to HAt, and reaches about 30% for HTs, though in absolute terms the differences are still modest. We note that our CCSD dipole moments compare well with available experimental<sup>143,144</sup> or theoretical work (for HTs),<sup>145</sup> though for reaching benchmark accuracy we would need to account for higher excitations, something which is beyond the scope of this work. These findings add to the body of data supporting the argument that differences between LR-CC and LR-EOMCC properties are in practice small.

Considering now the individual contributors to the value of the QR-CC functions, we see that dominant contributions typically arise from the terms from eq. 14b, involving both the perturbed amplitudes and multipliers ( $\overset{x}{t} \mathbf{A}^{Yz}$  and  $\overset{x}{t} \mathbf{B}^{yz}$ ). Furthermore, we observe that these two contributions to the final value in general tend to counteract each other, and that the magnitude of the “doubles” contributions increases as the halide becomes heavier. Terms from eq. 14a, involving only perturbed amplitudes and ground-state multipliers ( $\mathbf{F}^{Xyz}$  and  $\mathbf{G}^{xyz}$ ) show smaller (but non-negligible) net contributions than those above. They also increase in absolute value as the halide becomes heavier.

The relative importance of contribution of the terms in eq. 14b also changes depending on which response function we look at. For  $\langle\langle Z; Z, Z \rangle\rangle_0$ , the term  $\overset{x}{t} \mathbf{A}^{Yz}$  is the one which contributes the most, but for  $\langle\langle Z; X, X \rangle\rangle_0$  there are more important cancellations between the “singles” and “doubles” contributions from it so that the  $\overset{x}{t} \mathbf{B}^y$  term becomes a more important net contributor, being the dominant one for the HI molecule followed by  $\mathbf{F}^{Xyz}$ , whereas  $\overset{x}{t} \mathbf{A}^{Yz}$  and  $\mathbf{G}^{xyz}$  show similar contributions.

For QR-EOMCC, we see some similarities to the QR-CC picture, in that contributions beyond “singles” become increasingly important as the halogen becomes heavier, while the term  ${}^{\text{EOM}}\eta^X \mathbf{A}^{Yz}$  is typically a key contribution and dominates for the lightest elements. The value of the  ${}^{\text{EOM}}\eta^X \mathbf{A}^{Yz}$  contribution also appears to follow closely that of  $\overset{x}{t} \mathbf{A}^{Yz} + \overset{x}{t} \mathbf{B}^{yz}$  in QR-CC. The terms  $-\overset{xy}{t} \xi^Z$  and  $-\overset{yz}{t} \xi^X$ , on the other hand, become increasingly more important for heavier systems, and for  $\langle\langle Z; Z, Z \rangle\rangle_0$  of HBr and HI, they offset the other contribution

and are largely responsible for the sign changes between QR-CC and QR-EOMCC for these systems.

## Verdet constant of Xe, Rn and Og

In table 4 we present our results for the calculation of the Verdet constant for Xe, Rn and Og. In line with our prior work, we considered three laser wavelengths (589 nm, 694.3 nm, and 1064 nm) to compare QR-EOMCC and QR-CC for different Hamiltonians. The Verdet constants are evaluated as quadratic response functions:<sup>30,73</sup>

$$V(\omega) = \omega \frac{eN\epsilon_{xyz}}{24c_0\epsilon_0m_e} \text{Im}\langle\langle\hat{\mu}_x; \hat{\mu}_y, \hat{m}_z\rangle\rangle_{\omega,0} \quad (19)$$

with  $N$  the number density of the gas,  $e$  the elementary charge,  $m_e$  the electron mass,  $c_0$  the speed of light in vacuo, and  $\hat{m}_z$  is magnetic dipole moment operator. Given the atomic symmetry, we only needed to calculate one unique component and could obtain  $V(\omega)$  through the expression

$$V(\omega) = \omega \frac{eN}{4c_0\epsilon_0m_e} \text{Im}\langle\langle\hat{Y}; \hat{X}, \hat{m}_z\rangle\rangle_{\omega,0}. \quad (20)$$

Comparing first the differences between QR-CC and QR-EOMCC, we observe that these become larger as the wavelength decreases, and increase as well as the atoms become heavier. However, if we consider the magnitude of these differences, we see that the differences are rather small overall, between 1.1% and 1.3%, and are very similar for the different wavelengths. These additional calculations with respect to those already reported by,<sup>115</sup> allow us to more clearly separate contributions from different relativistic effects. With respect to the Hamiltonian and as discussed previously, the Verdet constant for Xe is still well described by non-relativistic Hamiltonians,<sup>115,146</sup> and scalar relativity is the dominant relativistic effect. Furthermore, we observe no difference between (SF-)X2C and (SF-)<sup>2</sup>DC<sup>M</sup> results, and find only rather small differences X2C and <sup>2</sup>DC<sup>M</sup>. As this is an atomic system, these differences are primarily due to the difference in Hamiltonian used to compute the spin-orbit screening

in the mean-field approximation used in the X2C approach. Adding the Gaunt interaction to this mean-field screening acts to slightly decrease the  ${}^2\text{DC}^M$  value, in the direction of the spinfree and X2C (Douglas-Kroll-Hess based screening) result. We also observe that in spite of the fact that QR-CC values are smaller than QR-EOMCC ones, they still overestimate the experimental results. For Rn relativistic effects are important and spin-orbit coupling effects significantly increase the Verdet constant. We again see some small differences between X2C and  ${}^2\text{DC}^M$ . For Og, spin-free results with X2C and  ${}^2\text{DC}^M$  are roughly the same, indicating that the bare nucleus and screened X2C transformation matrices are very similar (this is the only difference between the two spin-free approaches, see<sup>122</sup> for a more extensive discussion). With spin-orbit coupling differences between X2C and  ${}^2\text{DC}^M$  are more noticeable at about 3%. For this superheavy element, the spin-orbit effect is very significant and even dominates over scalar relativity, with  ${}^2\text{DC}^M$  values being roughly three times that of SF- ${}^2\text{DC}^M$ . While much larger in magnitude, the Gaunt interaction behaves similarly in Og as in Xe, reducing the Verdet constant at all frequencies.

In figure 4 we present the frequency dependence of the Verdet constant obtained with the  ${}^2\text{DC}^M$  Hamiltonian (see SI for the values for each atom at different frequencies). From these data, we observe that no significant discrepancy arises from the use of QR-EOMCC instead of QR-CC. Across the range of studied wave lengths, the differences are only of the order of 1.1-1.3 %. The magnitude of the Verdet constant for Rn is found to be roughly twice of that for Xe across the range of studied wavelenghts, while the one of Og is much larger still, with its magnitude being 4.5 times larger for the longest to about 6.5 times larger for the shortest wavelenghts. This is in stark contrast to what is observed for the spin-free calculation presented in table 4, where we see changes of only a factor of roughly 1.5 going from Xe to Rn, and of 1.8 going from Rn to Og. This is consistent with prior theoretical investigations of Og, that predict this element to be much more polarizable due to the extremely large spin-orbit effects in this superheavy element.<sup>147,148</sup> While the first excited state is lowered due to relativity, this strongly increased polarizability due to spin-

orbit effects manifests itself already far away from this resonance. To document this, we include in the SI calculations for the lowest excited states of these atoms. These show that while the first excited state is progressively lowered by spin-orbit coupling as the atom gets heavier, the wavelengths probed are still far away from the resonances.

Table 4: Verdet Constant  $V(\omega)$  [in  $10^{-3}$  rad/(T m)] for Gaseous Xe, Rn and Og at Different Laser Wavelengths, calculated with QR-CCSD (denoted by CC) and QR-EOMCCSD (denoted by EOM) upon correlating the  $nsnp$  shells (and with virtual threshold at 5 a.u.), as well as the difference in Verdet constant between the two approaches ( $\Delta V = V^{\text{CC}} - V^{\text{EOM}}$ ). For Xe, experimental values at  $\lambda(589 \text{ nm})$  and  $\lambda(1064 \text{ nm})$  are respectively  $12.30 \cdot 10^{-3}$  rad/(T m)<sup>149</sup> and  $3.56 \pm 0.10 \cdot 10^{-3}$  rad/(T m).<sup>146</sup>

Atom	Hamiltonian	$\lambda(589 \text{ nm})$			$\lambda(694.3 \text{ nm})$			$\lambda(1064 \text{ nm})$		
		CC	EOM	$\Delta V$	CC	EOM	$\Delta V$	CC	EOM	$\Delta V$
Xe	SF-X2C	12.39	12.54	-0.15	8.72	8.82	-0.11	3.60	3.64	-0.04
	SF- <sup>2</sup> DC <sup>M</sup>	12.40	12.55	-0.15	8.72	8.83	-0.11	3.60	3.64	-0.04
	X2C	12.95	13.10	-0.15	9.10	9.20	-0.11	3.74	3.79	-0.05
	<sup>2</sup> DC <sup>M</sup>	13.00	13.16	-0.15	9.14	9.24	-0.11	3.76	3.81	-0.05
	<sup>2</sup> DCG <sup>M</sup>	12.97	13.12	-0.15	9.11	9.22	-0.11	3.75	3.80	-0.05
Rn	SF-X2C	18.79	19.01	-0.22	13.14	13.30	-0.15	5.38	5.44	-0.06
	SF- <sup>2</sup> DC <sup>M</sup>	18.82	19.04	-0.22	13.16	13.31	-0.15	5.38	5.45	-0.06
	X2C	25.62	25.90	-0.28	17.73	17.92	-0.19	7.14	7.22	-0.08
	<sup>2</sup> DC <sup>M</sup>	26.07	26.35	-0.28	18.03	18.22	-0.20	7.26	7.34	-0.08
	<sup>2</sup> DCG <sup>M</sup>	25.95	26.24	-0.28	17.95	18.15	-0.20	7.23	7.31	-0.08
Og	SF-X2C	35.45	35.83	-0.38	24.44	24.71	-0.27	9.81	9.91	-0.11
	SF- <sup>2</sup> DC <sup>M</sup>	35.58	35.95	-0.38	24.53	24.79	-0.26	9.84	9.95	-0.11
	X2C	144.66	146.52	-1.85	92.02	93.20	-1.18	33.34	33.77	-0.43
	<sup>2</sup> DC <sup>M</sup>	151.00	152.95	-1.95	95.74	96.98	-1.24	34.55	35.00	-0.45
	<sup>2</sup> DCG <sup>M</sup>	149.96	151.92	-1.96	95.12	96.36	-1.24	34.34	34.79	-0.45

To further complete the picture, we computed the <sup>2</sup>DC<sup>M</sup> dipole polarizabilities for the noble gases with LR-CC and LR-EOMCC for the same range of frequencies as for the Verdet constant. The results, presented in the SI, are in line with the findings for the static polarizabilities for the HX systems and our work<sup>113</sup> in that there is no appreciable difference between the two CC variants for this property. Our results are in good agreement with the experimental static dipole polarizabilities for Xe and Rn (27.3 and 35.8 a.u. respectively),<sup>150,151</sup> and likewise for the theoretical predictions for Og (57.98 a.u.) of Smits and cowork-

ers.<sup>69</sup> Though we did not calculate values for atomic Ts, our results from HTs capture well the trend of decreasing polarizability from Ts to Og (76.3 to 57.98 a.u.)<sup>69</sup> predicted in that work. We attribute the observed discrepancies to the lack of higher excitations in CCSD.

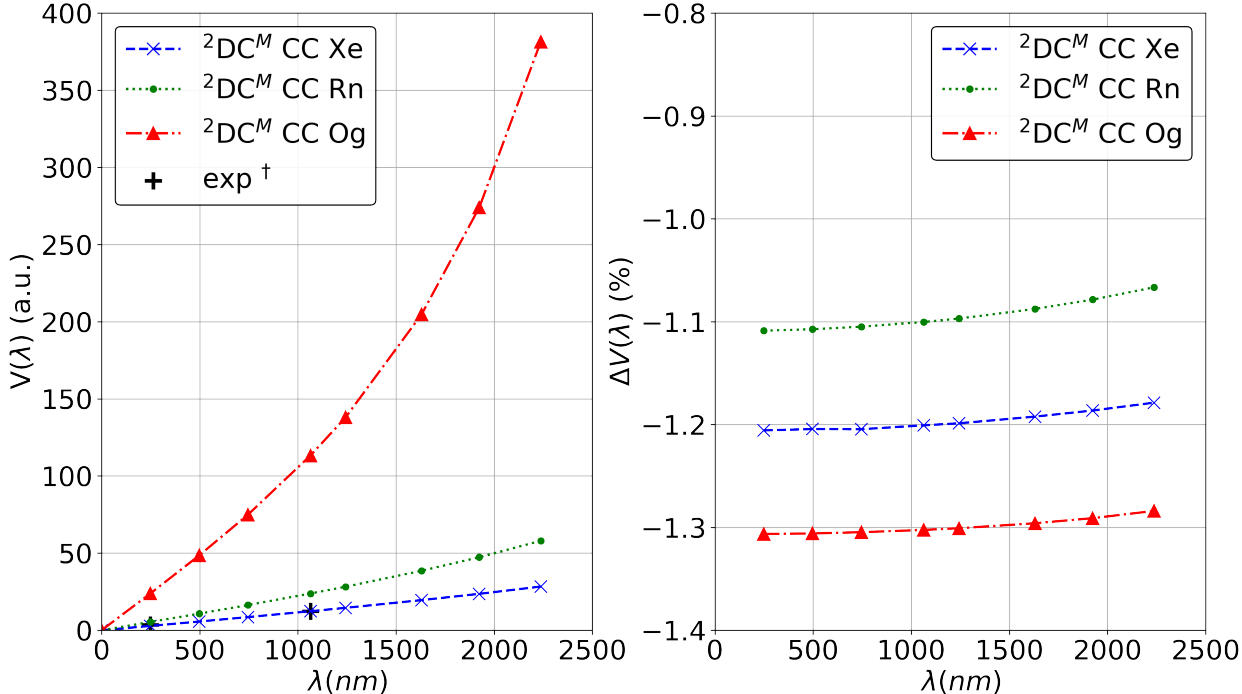


Figure 4: Left: frequency dependence of the QR-CC Verdet constants calculated with  $^2\text{DC}^M$  Hamiltonian for Xe, Rn and Og, upon correlating the  $(n - 1)nsnp$  shells (and with virtual threshold at 5 a.u.). <sup>†</sup> Experimental data from Ingersoll and Liebenberg<sup>149</sup> and Cadène et al.<sup>146</sup>. Right: frequency dependence of the difference between QR-CC and QR-EOMCC ( $\Delta V = (V_{CC} - V_{EOM})/V_{CC}$ , in %).

To check for the contribution of subvalence electrons, we also considered additional calculations in which we retained the virtual space truncation at 5 a.u. but included also the  $(n - 1)d$  electrons. In our prior QR-EOMCC calculations<sup>115</sup> we found, based on non-relativistic calculations (the difference of calculations with the same correlating space, and by correlating all occupied and virtual orbitals), that the effect of correlating electrons beyond the valence shell could result in a decrease of the Verdet constant by about  $-0.08 [10^{-3} \text{ rad}/(\text{T m})]$  for Xe. Our current results, shown in the SI, confirm that this trend is indeed followed by all atoms, though with the current virtual space truncation we only recover about half of this value. This change is consistent with our earlier finding, that upon cor-

relating the  $(n - 1)d$  electrons, the excitation energies for all systems are (slightly) shifted upward. Another change seen upon correlating the  $(n - 1)d$  electrons is that the difference between QR-CC and QR-EOMCC values increases somewhat, though in relative terms these differences remain close to 1% overall.

To conclude this section we note that, unlike the hyperpolarizability case, our results indicate that QR-CC and QR-EOMCC perform very much alike for the Verdet constant, and notably better than common density functional approximations such as B3LYP.<sup>115</sup> To keep computational costs manageable compared to such more approximate, but also much more efficient approaches, it may indeed be advantageous to resort to QR-EOMCC given its somewhat smaller memory footprint and cost as compared to QR-CC.

## Conclusions

In this work we have presented an implementation in the GPU-accelerated ExaCorr module of coupled cluster quadratic response (QR-CC) theory which can be used in combination with both (2- and 4-component based) relativistic and non-relativistic Hamiltonians, thus extending our prior implementation quadratic response based on the equation of motion (QR-EOMCC) formalism.<sup>115</sup>

We have showcased this implementation by carrying out a detailed comparison between QR-CC and QR-EOMCC in the calculation of both static and dynamic first hyperpolarizabilities for the hydrogen halide series (for HF to HTs), as well as the calculation of the Verdet constant for noble gases (Xe, Rn and Og). In addition to the comparison of non-relativistic and X2C Hamiltonians as done previously, we have carried out calculations with the X2C molecular mean field approach, and gauged the contribution of spin-orbit coupled and scalar relativistic effects.

For the first hyperpolarizabilities, we find that for the HF molecule the difference between QR-CC and EOM-CC is relatively small (around 4%), in line with the studies reported in

the literature employing non-relativistic approaches that do not see significant differences between the two approaches. The differences between QR-CC and QR-EOMCC do however increase as one goes down the periodic table, with differences of about 20% already for HCl and a sign change for  $\beta_{zzz}$  in HI. The overall shape of the dispersion curves remains unchanged, indicating that the EOM approximation yields qualitatively but not always quantitatively correct results. The contribution of spin-orbit coupling to the hyperpolarizability is rather small up to HBr, but becomes significant from HI onwards, also for the static case. Truncation of the correlating space appears to affect QR-EOMCC more than QR-CC for the  $\beta_{zzz}$  component for HBr, but the additional electron correlation recovered does not modify the trends upon going down the series from HF to HBr.

In contrast to the hyperpolarizabilities, for the Verdet constant the difference between QR-CC and EOM-CC is minor and roughly constant percentage-wise (about 1%) for all three systems studied. Spin-orbit coupling accounts for a relatively small part of the response (about 4%) in Xe, becomes important for Rn (about 35-40%) and absolutely dominates for Og. Correlating the  $(n - 1)d$  electrons in addition to the valence reduces the magnitude of the Verdet constants by about 10%.

The calculations presented here, albeit restricted to a relatively small set of atomic and molecular systems serve to highlight similarities, but also sometimes important differences, in behavior between the QR-CC and QR-EOMCC approaches across the periodic table and for different molecular properties. While QR-EOMCC is advantageous in terms of computational cost and implementation complexity with respect to QR-CC, it is thus important to further characterize differences between the two approaches in the calculation of nonlinear properties for heavier element systems.

## Acknowledgement

This research used resources of the Oak Ridge Leadership Computing Facility, which is a DOE Office of Science User Facility supported under Contract DE-AC05-00OR22725 (allocations CHM160, CHM191 and CHP109). XY, LH and ASPG acknowledge funding from projects CPER WaveTech, Labex CaPPA (Grant No. ANR-11-LABX-0005-01), ANR CompRIXS (Grant Nos. ANR-19-CE29-0019 and DFG JA 2329/6-1), ANR SCREECHES (Grant Nos. ANR-24-CE29-0904) the I-SITE ULNE project OVERSEE and MESONM International Associated Laboratory (LAI) (Grant No. ANR-16-IDEX-0004), as well support from the French national supercomputing facilities (Grant Nos. DARI A0150801859, A0170801859) and the HPC center at the University of Lille. For the purpose of Open Access, a CC-BY public copyright license has been applied by the authors to the present document and will be applied to all subsequent versions up to the Author Accepted Manuscript arising from this submission.

## Supporting Information Available

The data (input/output) corresponding to the calculations of this paper are available at the Zenodo repository under DOI: 10.5281/zenodo.15738821.

The Supporting Information is available free of charge on the ACS Publications website at DOI: XXX.

## References

- (1) Norman, P.; Ruud, K.; Saue, T. *Principles and practices of molecular properties: theory, modeling, and simulations*; Wiley: Hoboken, NJ, 2018.
- (2) Jaszunski, M.; Rizzo, A.; Ruud, K. *Handbook of Computational Chemistry*; Springer Netherlands, 2015; p 1–97.

- (3) Bishop, D. M. Molecular vibrational and rotational motion in static and dynamic electric fields. *Rev. Mod. Phys.* **1990**, *62*, 343–374.
- (4) Helgaker, T.; Jaszunski, M.; Ruud, K. Ab initio methods for the calculation of NMR shielding and indirect spin-spin coupling constants. *Chem. Rev* **1999**, *99*, 293–352.
- (5) Vaara, J. Theory and computation of nuclear magnetic resonance parameters. *Phys. Chem. Chem. Phys* **2007**, *9*, 5399–5418.
- (6) Helgaker, T.; Jaszunski, M.; Pecul, M. The quantum-chemical calculation of NMR indirect spin–spin coupling constants. *Prog. Nucl. Mag. Res. Sp* **2008**, *53*, 249.
- (7) Papadopoulos, M. G., Sadlej, A. J., Leszczynski, J., Eds. *Non-linear optical properties of matter: from molecules to condensed phases*; Springer, 2006.
- (8) He, G. S.; Tan, L.-S.; Zheng, Q.; Prasad, P. N. Multiphoton absorbing materials: molecular designs, characterizations, and applications. *Chem. Rev* **2008**, *108*, 1245–1330.
- (9) Norman, P.; Ruud, K. *Non-Linear Optical Properties of Matter*; Springer Netherlands, 2006; p 1–49.
- (10) Boyd, R. W. *Nonlinear optics*; Academic press, 2020.
- (11) Cronstrand, P.; Luo, Y.; Ågren, H. Multi-Photon Absorption of Molecules. *Adv. Quantum. Chem.* **2005**, *50*, 1–21.
- (12) Helgaker, T.; Coriani, S.; Jørgensen, P.; Kristensen, K.; Olsen, J.; Ruud, K. Recent Advances in Wave Function-Based Methods of Molecular-Property Calculations. *Chem. Rev.* **2012**, *112*, 543–631.
- (13) Helgaker, T.; Jørgensen, P.; Olsen, J. *Molecular Electronic-Structure Theory*; 2014; OCLC: 904835967.

- (14) Norman, P. A perspective on nonresonant and resonant electronic response theory for time-dependent molecular properties. *Phys. Chem. Chem. Phys.* **2011**, *13*, 20519.
- (15) Pedersen, T. B. *Handbook of Computational Chemistry*; Springer Netherlands, 2015; pp 1–26.
- (16) Dalgaard, E. Time-dependent multiconfigurational Hartree–Fock theory. *J. Chem. Phys* **1980**, *72*, 816–823.
- (17) Olsen, J.; Jørgensen, P. Linear and nonlinear response functions for an exact state and for an MCSCF state. *J. Chem. Phys* **1985**, *82*, 3235–3264.
- (18) Hettema, H.; Jensen, H. J. A.; Jørgensen, P.; Olsen, J. Quadratic response functions for a multiconfigurational self-consistent field wave function. *The Journal of Chemical Physics* **1992**, *97*, 1174–1190.
- (19) Casida, M. E. *Recent Developments and Applications of Modern Density Functional Theory*; Elsevier, 1996; p 391–439.
- (20) Koch, H.; Jørgensen, P. Coupled cluster response functions. *The Journal of Chemical Physics* **1990**, *93*, 3333–3344.
- (21) Koch, H.; Kobayashi, R.; de Merás, A. S.; Jørgensen, P. Calculation of size-intensive transition moments from the coupled cluster singles and doubles linear response function. *J. Chem. Phys* **1994**, *100*, 4393–4400.
- (22) Kobayashi, R.; Koch, H.; Jørgensen, P. Calculation of frequency-dependent polarizabilities using coupled-cluster response theory. *Chem. Phys. Lett* **1994**, *219*, 30–35.
- (23) Langhoff, P.; Epstein, S.; Karplus, M. Aspects of time-dependent perturbation theory. *Rev. Mod. Phys* **1972**, *44*, 602.
- (24) Rice, J. E.; Handy, N. C. The calculation of frequency-dependent polarizabilities as pseudo-energy derivatives. *J. Chem. Phys* **1991**, *94*, 4959–4971.

- (25) Sasagane, K.; Aiga, F.; Itoh, R. Higher-order response theory based on the quasienergy derivatives: The derivation of the frequency-dependent polarizabilities and hyperpolarizabilities. *J. Chem. Phys* **1993**, *99*, 3738–3778.
- (26) Christiansen, O.; Koch, H.; Jørgensen, P. The second-order approximate coupled cluster singles and doubles model CC2. *Chem. Phys. Lett* **1995**, *243*, 409–418.
- (27) Christiansen, O.; Koch, H.; Jørgensen, P. Response functions in the CC3 iterative triple excitation model. *The Journal of Chemical Physics* **1995**, *103*, 7429–7441.
- (28) Christiansen, O.; Koch, H.; Jørgensen, P.; Olsen, J. Excitation energies of H<sub>2</sub>O, N<sub>2</sub> and C<sub>2</sub> in full configuration interaction and coupled cluster theory. *Chemical Physics Letters* **1996**, *256*, 185–194.
- (29) Hättig, C.; Christiansen, O.; Koch, H.; Jørgensen, P. Frequency-dependent first hyperpolarizabilities using coupled cluster quadratic response theory. *Chemical Physics Letters* **1997**, *269*, 428–434.
- (30) Coriani, S.; Hättig, C.; Jørgensen, P.; Halkier, A.; Rizzo, A. Coupled cluster calculations of Verdet constants. *Chem. Phys. Lett* **1997**, *281*, 445–451.
- (31) Christiansen, O.; Jørgensen, P.; Hättig, C. Response functions from Fourier component variational perturbation theory applied to a time-averaged quasienergy. *Int. J. Quantum. Chem* **1998**, *68*, 1–52.
- (32) Gauss, J.; Christiansen, O.; Stanton, J. F. Triple excitation effects in coupled-cluster calculations of frequency-dependent hyperpolarizabilities. *Chemical Physics Letters* **1998**, *296*, 117–124.
- (33) Kauczor, J.; Norman, P.; Christiansen, O.; Coriani, S. Communication: A reduced-space algorithm for the solution of the complex linear response equations used in coupled cluster damped response theory. *J. Chem. Phys* **2013**, *139*, 211102.

- (34) Khani, S. K.; Faber, R.; Santoro, F.; Hättig, C.; Coriani, S. UV Absorption and Magnetic Circular Dichroism Spectra of Purine, Adenine, and Guanine: A Coupled Cluster Study in Vacuo and in Aqueous Solution. *J. Chem. Theory Comput.* **2019**, *15*, 1242–1254.
- (35) Hättig, C.; Weigend, F. CC2 excitation energy calculations on large molecules using the resolution of the identity approximation. *J. Chem. Phys.* **2000**, *113*, 5154–5161.
- (36) Höfener, S.; Severo Pereira Gomes, A.; Visscher, L. Molecular properties via a subsystem density functional theory formulation: A common framework for electronic embedding. *The Journal of Chemical Physics* **2012**, *136*.
- (37) Höfener, S.; Visscher, L. Calculation of electronic excitations using wave-function in wave-function frozen-density embedding. *The Journal of Chemical Physics* **2012**, *137*.
- (38) Höfener, S.; Gomes, A. S. P.; Visscher, L. Solvatochromic shifts from coupled-cluster theory embedded in density functional theory. *The Journal of Chemical Physics* **2013**, *139*.
- (39) Höfener, S.; Visscher, L. Wave Function Frozen-Density Embedding: Coupled Excitations. *Journal of Chemical Theory and Computation* **2016**, *12*, 549–557.
- (40) Niemeyer, N.; Neugebauer, J. Response properties from frozen-density embedding approximate second-order coupled-cluster theory. *The Journal of Chemical Physics* **2025**, *162*.
- (41) Myhre, R. H.; Sánchez de Merás, A. M. J.; Koch, H. Multi-level coupled cluster theory. *The Journal of Chemical Physics* **2014**, *141*.
- (42) Myhre, R. H.; Koch, H. The multilevel CC3 coupled cluster model. *The Journal of Chemical Physics* **2016**, *145*.

- (43) Goletto, L.; Giovannini, T.; Folkestad, S. D.; Koch, H. Combining multilevel Hartree–Fock and multilevel coupled cluster approaches with molecular mechanics: a study of electronic excitations in solutions. *Physical Chemistry Chemical Physics* **2021**, *23*, 4413–4425.
- (44) Stanton, J. F.; Bartlett, R. J. A coupled-cluster based effective Hamiltonian method for dynamic electric polarizabilities. *The Journal of Chemical Physics* **1993**, *99*, 5178–5183.
- (45) Stanton, J. F. Many-body methods for excited state potential energy surfaces. I. General theory of energy gradients for the equation-of-motion coupled-cluster method. *The Journal of Chemical Physics* **1993**, *99*, 8840–8847.
- (46) Sekino, H.; Bartlett, R. J. Frequency-dependent hyperpolarizabilities in the coupled-cluster method: the Kerr effect for molecules. *Chemical Physics Letters* **1995**, *234*, 87–93.
- (47) Gauss, J.; Stanton, J. F. Coupled-cluster calculations of nuclear magnetic resonance chemical shifts. *J. Chem. Phys* **1995**, *103*, 3561–3577.
- (48) Rozyczko, P.; Bartlett, R. J. Frequency dependent equation-of-motion coupled cluster hyperpolarizabilities: Resolution of the discrepancy between theory and experiment for HF? *The Journal of Chemical Physics* **1997**, *107*, 10823–10826.
- (49) Sekino, H.; Bartlett, R. J. *Advances in Quantum Chemistry*; Elsevier, 1999; pp 149–173.
- (50) Crawford, T. D.; Sekino, H. *Advances in the Theory of Atomic and Molecular Systems*; Springer Netherlands, 2009; pp 225–239.
- (51) Nanda, K. D.; Krylov, A. I. Two-photon absorption cross sections within equation-of-motion coupled-cluster formalism using resolution-of-the-identity and Cholesky de-

- composition representations: Theory, implementation, and benchmarks. *J. Chem. Phys* **2015**, *142*.
- (52) Nanda, K. D.; Krylov, A. I. Static polarizabilities for excited states within the spin-conserving and spin-flipping equation-of-motion coupled-cluster singles and doubles formalism: Theory, implementation, and benchmarks. *J. Chem. Phys* **2016**, *145*, 204116.
- (53) Nanda, K. D.; Krylov, A. I.; Gauss, J. Communication: The pole structure of the dynamical polarizability tensor in equation-of-motion coupled-cluster theory. *J. Chem. Phys* **2018**, *149*, 141101.
- (54) Stanton, J. F. Separability properties of reduced and effective density matrices in the equation-of-motion coupled cluster method. *The Journal of Chemical Physics* **1994**, *101*, 8928–8937.
- (55) Caricato, M.; Trucks, G. W.; Frisch, M. J. On the difference between the transition properties calculated with linear response-and equation of motion-CCSD approaches. *J. Chem. Phys* **2009**, *131*, 174104.
- (56) Pawłowski, F.; Olsen, J.; Jørgensen, P. Molecular response properties from a Hermitian eigenvalue equation for a time-periodic Hamiltonian. *J. Chem. Phys* **2015**, *142*, 114109.
- (57) Coriani, S.; Pawłowski, F.; Olsen, J.; Jørgensen, P. Molecular response properties in equation of motion coupled cluster theory: A time-dependent perspective. *J. Chem. Phys* **2016**, *144*, 024102.
- (58) Faber, R.; Coriani, S. Resonant inelastic X-ray scattering and nonresonant X-ray emission spectra from coupled-cluster (damped) response theory. *J. Chem. Theory. Comput* **2018**, *15*, 520–528.

- (59) Andersen, J. H.; Nanda, K. D.; Krylov, A. I.; Coriani, S. Cherry-picking resolvents: Recovering the valence contribution in X-ray two-photon absorption within the core-valence-separated equation-of-motion coupled-cluster response theory. *J. Chem. Theory. Comput* **2022**, *18*, 6189–6202.
- (60) Andersen, J. H.; Nanda, K. D.; Krylov, A. I.; Coriani, S. Probing Molecular Chirality of Ground and Electronically Excited States in the UV-vis and X-ray Regimes: An EOM-CCSD Study. *J. Chem. Theory. Comput* **2022**, *18*, 1748–1764.
- (61) Sekino, H.; Bartlett, R. J. Nuclear coupling constants obtained by the equation-of-motion coupled cluster theory. *Chem. Phys. Lett* **1994**, *225*, 486–493.
- (62) Širůček, J.; Le Guennic, B.; Damour, Y.; Loos, P.-F.; Jacquemin, D. Excited-State Absorption: Reference Oscillator Strengths, Wave Function, and TDDFT Benchmarks. *Journal of Chemical Theory and Computation* **2025**, *21*, 4688–4703.
- (63) Pyykko, P. Relativistic effects in structural chemistry. *Chemical Reviews* **1988**, *88*, 563–594.
- (64) Saue, T. Relativistic Hamiltonians for Chemistry: A Primer. *ChemPhysChem* **2011**, *12*, 3077–3094.
- (65) Pyykkö, P. Relativistic Effects in Chemistry: More Common Than You Thought. *Annual Review of Physical Chemistry* **2012**, *63*, 45–64.
- (66) Autschbach, J. Perspective: Relativistic effects. *The Journal of Chemical Physics* **2012**, *136*.
- (67) Liu, W. *Handbook of relativistic quantum chemistry*; Springer Berlin Heidelberg Berlin, Heidelberg, 2017.
- (68) Schwerdtfeger, P.; Smits, O. R.; Pyykkö, P. The periodic table and the physics that drives it. *Nature Reviews Chemistry* **2020**, *4*, 359–380.

- (69) Smits, O.; Indelicato, P.; Nazarewicz, W.; Piibeleht, M.; Schwerdtfeger, P. Pushing the limits of the periodic table — A review on atomic relativistic electronic structure theory and calculations for the superheavy elements. *Physics Reports* **2023**, *1035*, 1–57.
- (70) Saue, T. *Theoretical and Computational Chemistry*; Elsevier, 2002; pp 332–400.
- (71) Visscher, L.; Saue, T.; Oddershede, J. The 4-component random phase approximation method applied to the calculation of frequency-dependent dipole polarizabilities. *Chem. Phys. Lett* **1997**, *274*, 181–188.
- (72) Saue, T.; Jensen, H. J. Aa. Linear response at the 4-component relativistic level: Application to the frequency-dependent dipole polarizabilities of the coinage metal dimers. *J. Chem. Phys.* **2003**, *118*, 522–536.
- (73) Norman, P.; Jensen, H. J. A. Quadratic response functions in the time-dependent four-component Hartree-Fock approximation. *J. Chem. Phys.* **2004**, *121*, 6145–6154.
- (74) Sałek, P.; Helgaker, T.; Saue, T. Linear response at the 4-component relativistic density-functional level: application to the frequency-dependent dipole polarizability of Hg, AuH and PtH<sub>2</sub>. *Chem. Phys* **2005**, *311*, 187–201.
- (75) Henriksson, J.; Norman, P.; Jensen, H. J. Aa. Two-photon absorption in the relativistic four-component Hartree-Fock approximation. *J. Chem. Phys.* **2005**, *122*, 114106.
- (76) Henriksson, J.; Ekström, U.; Norman, P. On the evaluation of quadratic response functions at the four-component Hartree-Fock level: Nonlinear polarization and two-photon absorption in bromo- and iodobenzene. *J. Chem. Phys.* **2006**, *124*, 214311.
- (77) Tellgren, E.; Henriksson, J.; Norman, P. First-order excited state properties in the four-component Hartree-Fock approximation: The excited state electric dipole moments in CsAg and CsAu. *J. Chem. Phys.* **2007**, *126*, 064313.

- (78) Bast, R.; Saue, T.; Henriksson, J.; Norman, P. Role of noncollinear magnetization for the first-order electric-dipole hyperpolarizability at the four-component Kohn–Sham density functional theory level. *J. Chem. Phys.* **2009**, *130*, 024109.
- (79) Bast, R.; Jensen, H. J. Aa.; Saue, T. Relativistic adiabatic time-dependent density functional theory using hybrid functionals and noncollinear spin magnetization. *Int. J. Quantum Chem.* **2009**, *109*, 2091–2112.
- (80) Bast, R.; Thorvaldsen, A. J.; Ringholm, M.; Ruud, K. Atomic orbital-based cubic response theory for one-, two-, and four-component relativistic self-consistent field models. *Chemical Physics* **2009**, *356*, 177–186.
- (81) Villaume, S.; Saue, T.; Norman, P. Linear complex polarization propagator in a four-component Kohn–Sham framework. *J. Chem. Phys.* **2010**, *133*, 064105.
- (82) Liu, J.; Cheng, L. Relativistic coupled-cluster and equation-of-motion coupled-cluster methods. *WIREs Computational Molecular Science* **2021**, *11*.
- (83) Visscher, L.; Lee, T. J.; Dyall, K. G. Formulation and implementation of a relativistic unrestricted coupled-cluster method including noniterative connected triples. *J. Chem. Phys* **1996**, *105*, 8769–8776.
- (84) Pototschnig, J. V.; Papadopoulos, A.; Lyakh, D. I.; Repisky, M.; Halbert, L.; Severo Pereira Gomes, A.; Jensen, H. J. A.; Visscher, L. Implementation of Relativistic Coupled Cluster Theory for Massively Parallel GPU-Accelerated Computing Architectures. *J. Chem. Theory Comput.* **2021**, acs.jctc.1c00260.
- (85) Yuwono, S. H.; Li, R. R.; Zhang, T.; Surjuse, K. A.; Valeev, E. F.; Li, X.; Eugene DePrince, A. Relativistic Coupled Cluster with Completely Renormalized and Perturbative Triples Corrections. *The Journal of Physical Chemistry A* **2024**, *128*, 6521–6539.

- (86) Chamoli, S.; Wang, X.; Zhang, C.; Nayak, M. K.; Dutta, A. K. Frozen Natural Spinors for Cholesky Decomposition-Based Two-Component Relativistic Coupled Cluster Method. *Journal of Chemical Theory and Computation* **2025**, *21*, 4532–4542.
- (87) Brandejs, J.; Pototschnig, J.; Saue, T. Generating coupled cluster code for modern distributed memory tensor software. 2024; <https://arxiv.org/abs/2409.06759>.
- (88) Pathak, H.; Sasmal, S.; Nayak, M. K.; Vaval, N.; Pal, S. Relativistic equation-of-motion coupled-cluster method for the electron attachment problem. *Comput. Theor. Chem.* **2016**, *1076*, 94–100.
- (89) Pathak, H.; Sahoo, B. K.; Sengupta, T.; Das, B. P.; Vaval, N.; Pal, S. A relativistic equation-of-motion coupled-cluster investigation of the trends of single and double ionization potentials in the He and Be isoelectronic systems. *J. Phys. B: Atom. Mol. Opt. Phys.* **2015**, *48*, 115009–10.
- (90) Pathak, H.; Sasmal, S.; Nayak, M. K.; Vaval, N.; Pal, S. Relativistic equation-of-motion coupled-cluster method for the ionization problem: Application to molecules. *Phys. Rev. A* **2014**, *90*, 062501–7.
- (91) Pathak, H.; Sahoo, B. K.; Das, B. P.; Vaval, N.; Pal, S. Relativistic equation-of-motion coupled-cluster method: Application to closed-shell atomic systems. *Phys. Rev. A* **2014**, *89*, 042510–7.
- (92) Pathak, H.; Sasmal, S.; Nayak, M. K.; Vaval, N.; Pal, S. Relativistic equation-of-motion coupled-cluster method using open-shell reference wavefunction: Application to ionization potential. *J. Chem. Phys.* **2016**, *145*, 074110–8.
- (93) Klein, K.; Gauss, J. Perturbative calculation of spin-orbit splittings using the equation-of-motion ionization-potential coupled-cluster ansatz. *J. Chem. Phys.* **2008**, *129*, 194106–7.

- (94) Yang, D.-D.; Wang, F.; Guo, J. Equation of motion coupled cluster method for electron attached states with spin-orbit coupling. *Chem. Phys. Lett.* **2012**, *531*, 236–241.
- (95) Wang, Z.; Hu, S.; Wang, F.; Guo, J. Equation-of-motion coupled-cluster method for doubly ionized states with spin-orbit coupling. *J. Chem. Phys.* **2015**, *142*, 144109–10.
- (96) Epifanovsky, E.; Klein, K.; Stopkowicz, S.; Gauss, J.; Krylov, A. I. Spin-orbit couplings within the equation-of-motion coupled-cluster framework: Theory, implementation, and benchmark calculations. *J. Chem. Phys.* **2015**, *143*, 064102–17.
- (97) Cao, Z.; Wang, F.; Yang, M. Spin-orbit coupling with approximate equation-of-motion coupled-cluster method for ionization potential and electron attachment. *J. Chem. Phys.* **2016**, *145*, 154110–13.
- (98) Cao, Z.; Li, Z.; Wang, F.; Liu, W. Combining spin-separated exact two-component relativistic Hamiltonian with equation-of-motion coupled-cluster for spin-orbit splittings of light and heavy elements. *Phys. Chem. Chem. Phys.* **2017**, *19*, 3713–3721.
- (99) Zhang, S.; Wang, F. Excitation Energies of UO 22+, NUO +, and NUN Based on Equation-of-Motion Coupled-Cluster Theory with Spin–Orbit Coupling. *J. Phys. Chem. A* **2017**, *121*, 3966–3975.
- (100) Akinaga, Y.; Nakajima, T. Two-Component Relativistic Equation-of-Motion Coupled-Cluster Methods for Excitation Energies and Ionization Potentials of Atoms and Molecules. *J. Phys. Chem. A* **2017**, *121*, 827–835.
- (101) Wang, F. In *Handbook of Relativistic Quantum Chemistry*; Liu, W., Ed.; Springer Berlin Heidelberg: Berlin, Heidelberg, 2016; pp 1–27.
- (102) Shee, A.; Saue, T.; Visscher, L.; Severo Pereira Gomes, A. Equation-of-motion coupled-cluster theory based on the 4-component Dirac–Coulomb (–Gaunt) Hamilto-

- nian. Energies for single electron detachment, attachment, and electronically excited states. *J. Chem. Phys* **2018**, *149*, 174113.
- (103) Koulias, L. N.; Williams-Young, D. B.; Nascimento, D. R.; DePrince, A. E.; Li, X. Relativistic Real-Time Time-Dependent Equation-of-Motion Coupled-Cluster. *Journal of Chemical Theory and Computation* **2019**, *15*, 6617–6624.
- (104) Halbert, L.; Vidal, M. L.; Shee, A.; Coriani, S.; Gomes, A. S. P. Relativistic EOM-CCSD for Core-Excited and Core-Ionized State Energies Based on the Four-Component Dirac–Coulomb(-Gaunt) Hamiltonian. *Journal of Chemical Theory and Computation* **2021**, *17*, 3583–3598.
- (105) Halbert, L.; Gomes, A. S. P. The performance of approximate equation of motion coupled cluster for valence and core states of heavy element systems. *Molecular Physics* **2023**, *123*.
- (106) Zhang, T.; Banerjee, S.; Koulias, L. N.; Valeev, E. F.; DePrince, A. E.; Li, X. Dirac–Coulomb–Breit Molecular Mean-Field Exact-Two-Component Relativistic Equation-of-Motion Coupled-Cluster Theory. *The Journal of Physical Chemistry A* **2024**, *128*, 3408–3418.
- (107) Zhang, C.; Lipparini, F.; Stopkowicz, S.; Gauss, J.; Cheng, L. Cholesky Decomposition-Based Implementation of Relativistic Two-Component Coupled-Cluster Methods for Medium-Sized Molecules. *Journal of Chemical Theory and Computation* **2024**, *20*, 787–798.
- (108) Uhlířová, T.; Cianchino, D.; Nottoli, T.; Lipparini, F.; Gauss, J. Cholesky Decomposition in Spin-Free Dirac–Coulomb Coupled-Cluster Calculations. *The Journal of Physical Chemistry A* **2024**, *128*, 8292–8303.
- (109) Yuwono, S. H.; Li, R. R.; Zhang, T.; Li, X.; DePrince, A. E. Two-component relativis-

- tic equation-of-motion coupled cluster for electron ionization. *The Journal of Chemical Physics* **2025**, *162*.
- (110) Li, R. R.; Yuwono, S. H.; Liebenthal, M. D.; Zhang, T.; Li, X.; DePrince, A. E. Relativistic Two-component Double Ionization Potential Equation-of-Motion Coupled Cluster with the Dirac–Coulomb–Breit Hamiltonian. 2025; <https://arxiv.org/abs/2505.00499>.
- (111) Banerjee, S.; Li, R. R.; Cooper, B. C.; Zhang, T.; Valeev, E. F.; Li, X.; DePrince, A. E. Relativistic Core-Valence-Separated Molecular Mean-Field Exact-Two-Component Equation-of-Motion Coupled Cluster Theory: Applications to L-edge X-ray Absorption Spectroscopy. 2025; <https://arxiv.org/abs/2506.09008>.
- (112) Mukhopadhyay, T.; Chakraborty, S.; Chamoli, S.; Nayak, M. K.; Dutta, A. K. Analytic calculation of transition dipole moment using four-component relativistic equation-of-motion coupled-cluster expectation value approach. *The Journal of Chemical Physics* **2025**, *162*.
- (113) Yuan, X.; Halbert, L.; Pototschnig, J. V.; Papadopoulos, A.; Coriani, S.; Visscher, L.; Pereira Gomes, A. S. Formulation and Implementation of Frequency-Dependent Linear Response Properties with Relativistic Coupled Cluster Theory for GPU-Accelerated Computer Architectures. *Journal of Chemical Theory and Computation* **2024**, *20*, 677–694.
- (114) Chakraborty, S.; Mukhopadhyay, T.; Dutta, A. K. Spin-Free Exact Two-Component Linear Response Coupled Cluster Theory for the Estimation of Frequency-Dependent Second-Order Properties. *The Journal of Physical Chemistry A* **2025**, *129*, 3315–3330.
- (115) Yuan, X.; Halbert, L.; Visscher, L.; Pereira Gomes, A. S. Frequency-Dependent Quadratic Response Properties and Two-Photon Absorption from Relativistic

- Equation-of-Motion Coupled Cluster Theory. *Journal of Chemical Theory and Computation* **2023**, *19*, 9248–9259.
- (116) Karol, P. J.; Barber, R. C.; Sherrill, B. M.; Vardaci, E.; Yamazaki, T. Discovery of the elements with atomic numbers  $Z=113$ , 115 and 117 (IUPAC Technical Report). *Pure and Applied Chemistry* **2016**, *88*, 139–153.
- (117) Karol, P. J.; Barber, R. C.; Sherrill, B. M.; Vardaci, E.; Yamazaki, T. Discovery of the element with atomic number  $Z = 118$  completing the 7th row of the periodic table (IUPAC Technical Report). *Pure and Applied Chemistry* **2016**, *88*, 155–160.
- (118) Smits, O. R.; Düllmann, C. E.; Indelicato, P.; Nazarewicz, W.; Schwerdtfeger, P. The quest for superheavy elements and the limit of the periodic table. *Nature Reviews Physics* **2023**, *6*, 86–98.
- (119) Liu, W.; Lindgren, I. Going beyond “no-pair relativistic quantum chemistry”. *The Journal of Chemical Physics* **2013**, *139*, 014108.
- (120) Almoukhalalati, A.; Knecht, S.; Jensen, H. J. A.; Dyllal, K. G.; Saue, T. Electron correlation within the relativistic no-pair approximation. *The Journal of Chemical Physics* **2016**, *145*, 074104.
- (121) Schimmelpfennig, B.; Maron, L.; Wahlgren, U.; Teichteil, C.; Fagerli, H.; Gropen, O. On the combination of ECP-based CI calculations with all-electron spin-orbit mean-field integrals. *Chem. Phys. Lett* **1998**, *286*, 267 – 271.
- (122) Sikkema, J.; Visscher, L.; Saue, T.; Iliáš, M. The molecular mean-field approach for correlated relativistic calculations. *J. Chem. Phys* **2009**, *131*, 124116.
- (123) Iliáš, M.; Saue, T. An infinite-order two-component relativistic Hamiltonian by a simple one-step transformation. *J. Chem. Phys* **2007**, *126*, 064102.

- (124) Saue, T.; Helgaker, T. Four-component relativistic Kohn–Sham theory. *J. Comput. Chem* **2002**, *23*, 814–823.
- (125) Shavitt, I.; Bartlett, R. *Many-Body Methods in Chemistry and Physics: MBPT and Coupled-Cluster Theory*; Cambridge Molecular Science; Cambridge University Press, 2009.
- (126) Bartlett, R. J.; Musiał, M. Coupled-cluster theory in quantum chemistry. *Rev. Mod. Phys* **2007**, *79*, 291.
- (127) Saue, T.; Bast, R.; Gomes, A. S. P.; Jensen, H. J. A.; Visscher, L.; Aucar, I. A.; Di Remigio, R.; Dyall, K. G.; Eliav, E.; Fasshauer, E.; others The DIRAC code for relativistic molecular calculations. *J. Chem. Phys* **2020**, *152*, 204104.
- (128) Hirao, K.; Nakatsuji, H. A generalization of the Davidson’s method to large nonsymmetric eigenvalue problems. *J. Comput. Phys* **1982**, *45*, 246–254.
- (129) Olsen, J.; Jensen, H. J. A.; Jørgensen, P. Solution of the large matrix equations which occur in response theory. *J. Comput. Phys* **1988**, *74*, 265–282.
- (130) Lyakh, D. I. TAL-SH: Tensor Algebra Library for Shared Memory Computers. [github.com/https://DmitryLyakh/TAL\\_SH](https://github.com/DmitryLyakh/TAL_SH), 2023.
- (131) Lyakh, D. I. Domain-specific virtual processors as a portable programming and execution model for parallel computational workloads on modern heterogeneous high-performance computing architectures. *Int J Quantum Chem* **2019**, *119*, e25926.
- (132) DIRAC, a relativistic ab initio electronic structure program, Release DIRAC25 (2025), written by T. Saue, L. Visscher, H. J. Aa. Jensen, R. Bast and A. S. P. Gomes, with contributions from I. A. Aucar, V. Bakken, J. Brandejs, C. Chibueze, J. Creutzberg, K. G. Dyall, S. Dubillard, U. Ekström, E. Eliav, T. Enevoldsen, E. Faßhauer, T. Fleig, O. Fossgaard, K. G. Gaul, L. Halbert, E. D. Hedegård, T. Helgaker, B. Helmich–Paris,

- J. Henriksson, M. van Horn, M. Iliáš, Ch. R. Jacob, S. Knecht, S. Komorovský, O. Kullie, J. K. Lærdahl, C. V. Larsen, Y. S. Lee, N. H. List, H. S. Nataraj, M. K. Nayak, P. Norman, A. Nyvang, G. Olejniczak, J. Olsen, J. M. H. Olsen, A. Papadopoulos, Y. C. Park, J. K. Pedersen, M. Pernpointner, J. V. Pototschnig, R. di Remigio, M. Repisky, C. M. R. Rocha, K. Ruud, P. Salek, B. Schimmelpfennig, B. Senjean, A. Shee, J. Sikkema, A. Sunaga, A. J. Thorvaldsen, J. Thyssen, J. van Stralen, M. L. Vidal, S. Villaume, O. Visser, T. Winther, S. Yamamoto and X. Yuan (available at <https://doi.org/10.5281/zenodo.14833106>, see also <https://www.diracprogram.org>).
- (133) Kendall, R. A.; Dunning Jr, T. H.; Harrison, R. J. Electron affinities of the first-row atoms revisited. Systematic basis sets and wave functions. *J. Chem. Phys* **1992**, *96*, 6796–6806.
- (134) Woon, D. E.; Dunning Jr, T. H. Gaussian basis sets for use in correlated molecular calculations. III. The atoms aluminum through argon. *J. Chem. Phys* **1993**, *98*, 1358–1371.
- (135) Wilson, A. K.; Woon, D. E.; Peterson, K. A.; Dunning Jr, T. H. Gaussian basis sets for use in correlated molecular calculations. IX. The atoms gallium through krypton. *J. Chem. Phys* **1999**, *110*, 7667–7676.
- (136) Lévy-Leblond, J.-M. Nonrelativistic particles and wave equations. *Commun. Math. Phys* **1967**, *6*, 286–311.
- (137) Visscher, L.; Saue, T. Approximate relativistic electronic structure methods based on the quaternion modified Dirac equation. *J. Chem. Phys* **2000**, *113*, 3996–4002.
- (138) Visscher, L.; Dyall, K. G. Dirac–Fock atomic electronic structure calculations using different nuclear charge distributions. *Atom. Data. Nucl. Data* **1997**, *67*, 207–224.

- (139) Huber, K. P.; Herzberg, G. *Molecular Spectra and Molecular Structure*; Springer New York, NY, 1979.
- (140) Gomes, A. S. P.; Visscher, L. The influence of core correlation on the spectroscopic constants of HAt. *Chem. Phys. Lett.* **2004**, *399*, 1.
- (141) de Farias, R. F. Estimation of some physical properties for tennessine and tennessine hydride (TsH). *Chemical Physics Letters* **2017**, *667*, 1–3.
- (142) Shelton, D. P.; Rice, J. E. Measurements and calculations of the hyperpolarizabilities of atoms and small molecules in the gas phase. *Chem. Rev.* **1994**, *94*, 3–29.
- (143) Lovas, F. *Diatomic Spectral Database, NIST Standard Reference Database 114*; National Institute of Standards and Technology, 2002.
- (144) Hohm, U. Experimental static dipole–dipole polarizabilities of molecules. *Journal of Molecular Structure* **2013**, *1054–1055*, 282–292.
- (145) Thierfelder, C.; Schwerdtfeger, P.; Koers, A.; Borschevsky, A.; Fricke, B. Scalar relativistic and spin-orbit effects in closed-shell superheavy-element monohydrides. *Phys. Rev. A* **2009**, *80*, 022501.
- (146) Cadène, A.; Fouché, M.; Rivère, A.; Battesti, R.; Coriani, S.; Rizzo, A.; Rizzo, C. Circular and linear magnetic birefringences in xenon at  $\lambda = 1064$  nm. *J. Chem. Phys.* **2015**, *142*, 124313.
- (147) Jerabek, P.; Smits, O. R.; Mewes, J.-M.; Peterson, K. A.; Schwerdtfeger, P. Solid Oganesson via a Many-Body Interaction Expansion Based on Relativistic Coupled-Cluster Theory and from Plane-Wave Relativistic Density Functional Theory. *The Journal of Physical Chemistry A* **2019**, *123*, 4201–4211.
- (148) Jerabek, P.; Smits, O. R.; Mewes, J.-M.; Peterson, K. A.; Schwerdtfeger, P. Correction to “Solid Oganesson via a Many-Body Interaction Expansion Based on Rela-

- tivistic Coupled-Cluster Theory and from Plane-Wave Relativistic Density Functional Theory”. *The Journal of Physical Chemistry A* **2019**, *123*, 8333–8333.
- (149) Ingersoll, L. R.; Liebenberg, D. H. Faraday Effect in Gases and Vapors. II\*. *J. Opt. Soc. Am.* **1956**, *46*, 538–542.
- (150) Hohm, U.; Trümper, U. Temperature dependence of the dipole polarizability of xenon (1S0) due to dynamic non-resonant Stark effect caused by black-body radiation. *Chemical Physics* **1994**, *189*, 443–449.
- (151) *CRC Handbook of Chemistry and Physics*; CRC Press, 2014.

# Supplementary information: A Comparison of Relativistic Coupled Cluster and Equation of Motion Coupled Cluster Quadratic Response Theory

Xiang Yuan,<sup>†,‡</sup> Loïc Halbert,<sup>†</sup> Lucas Visscher,<sup>¶</sup> and André Severo Pereira  
Gomes<sup>\*,†</sup>

<sup>†</sup>*Univ. Lille, CNRS, UMR 8523 - PhLAM - Physique des Lasers Atomes et Molécules,  
F-59000 Lille, France*

<sup>‡</sup>*Department of Chemistry and Pharmaceutical Sciences, Faculty of Science, Vrije  
Universiteit Amsterdam, 1081 HZ Amsterdam, The Netherlands*

<sup>¶</sup>*Department of Chemistry and Pharmaceutical Sciences, Faculty of Science, Vrije  
Universiteit Amsterdam, 1081 Hz Amsterdam, The Netherlands*

E-mail: andre.gomes@univ-lille.fr

# Working equations for CCSD quadratic response

In the quadratic response function,<sup>1</sup>

$$\begin{aligned} \langle\langle X; Y, Z \rangle\rangle_{\omega_Z; \omega_X, \omega_Y} &= \frac{1}{2} C^{\pm\omega} P' (X(\omega_X), Y(\omega_Y), Z(\omega_Z)) \\ &\times \left\{ \left[ \frac{1}{2} \mathbf{F}^X + \frac{1}{6} \mathbf{G}^x t(\omega_X) \right]^y t(\omega_Y) + \bar{t}^x(\omega_X) \left[ \mathbf{A}^Y + \frac{1}{2} \mathbf{B}^y t(\omega_Y) \right] \right\}^z t(\omega_Z) \end{aligned} \quad (1)$$

we have that, with the exception of  $\mathbf{G}^{xyz}$ , all other terms can be obtained by adapting the working equations reported previously<sup>2</sup> and the respective computer implementations.

Employing Einstein notation, for  $\mathbf{G}^{xyz}$  the programmable expressions for are:

$$\begin{aligned} \left( G_{tt}^{xy} \right)_e^m &= -\bar{t}_c^i (V_{ae}^{km}) \cdot \bar{t}_i^a \cdot \bar{t}_k^c - \bar{t}_a^k (V_{ce}^{im}) \cdot \bar{t}_i^a \cdot \bar{t}_k^c - \bar{t}_e^k (V_{ca}^{mi}) \cdot \bar{t}_i^a \cdot \bar{t}_k^c \\ &- \bar{t}_e^i (V_{ac}^{mk}) \cdot \bar{t}_i^a \cdot \bar{t}_k^c - \bar{t}_c^m (V_{ea}^{ki}) \cdot \bar{t}_i^a \cdot \bar{t}_k^c - \bar{t}_a^m (V_{ec}^{ik}) \cdot \bar{t}_i^a \cdot \bar{t}_k^c \\ &+ \bar{t}_{ae}^{nk} (V_{nc}^{im}) \cdot \bar{t}_i^a \cdot \bar{t}_k^c - \bar{t}_{fa}^{mk} (V_{ec}^{fi}) \cdot \bar{t}_i^a \cdot \bar{t}_k^c - \bar{t}_{fc}^{im} (V_{ae}^{fk}) \cdot \bar{t}_i^a \cdot \bar{t}_k^c \\ &+ \bar{t}_{ec}^{mi} (V_{na}^{mk}) \cdot \bar{t}_i^a \cdot \bar{t}_k^c - \bar{t}_{fe}^{ik} (V_{ac}^{fm}) \cdot \bar{t}_i^a \cdot \bar{t}_k^c + \bar{t}_{ac}^{nm} (V_{ne}^{ik}) \cdot \bar{t}_i^a \cdot \bar{t}_k^c \\ &+ \bar{t}_{ae}^{ko} (V_{cg}^{im} t_o) \cdot \bar{t}_i^a \cdot \bar{t}_k^c + \bar{t}_{cf}^{im} (V_{ae}^{ko} t_o) \cdot \bar{t}_i^a \cdot \bar{t}_k^c \\ &+ \bar{t}_{eg}^{ki} (V_{ca}^{mo} t_o) \cdot \bar{t}_i^a \cdot \bar{t}_k^c + \bar{t}_{ca}^{mo} (V_{eg}^{ki} t_o) \cdot \bar{t}_i^a \cdot \bar{t}_k^c \\ &+ \bar{t}_{ce}^{io} (V_{ag}^{km} t_o) \cdot \bar{t}_i^a \cdot \bar{t}_k^c + \bar{t}_{ag}^{km} (V_{ce}^{io} t_o) \cdot \bar{t}_i^a \cdot \bar{t}_k^c \\ &- \frac{1}{2} \bar{t}_{bc}^{ji} (V_{ae}^{km}) \cdot \bar{t}_{ij}^{ab} \cdot \bar{t}_k^c - \frac{1}{2} \bar{t}_{ba}^{jk} (V_{ce}^{im}) \cdot \bar{t}_{ij}^{ab} \cdot \bar{t}_k^c - \frac{1}{2} \bar{t}_{eb}^{ij} (V_{ac}^{mk}) \cdot \bar{t}_{ij}^{ab} \cdot \bar{t}_k^c \\ &- \frac{1}{2} \bar{t}_{ba}^{jm} (V_{ec}^{ik}) \cdot \bar{t}_{ij}^{ab} \cdot \bar{t}_k^c + \frac{1}{4} \bar{t}_{ce}^{ij} (V_{ab}^{km}) \cdot \bar{t}_{ij}^{ab} \cdot \bar{t}_k^c + \frac{1}{4} \bar{t}_{ab}^{km} (V_{ce}^{ij}) \cdot \bar{t}_{ij}^{ab} \cdot \bar{t}_k^c \\ &- \bar{t}_{be}^{jk} (V_{ac}^{im}) \cdot \bar{t}_{ij}^{ab} \cdot \bar{t}_k^c - \bar{t}_{bc}^{jm} (V_{ae}^{ik}) \cdot \bar{t}_{ij}^{ab} \cdot \bar{t}_k^c \\ &- \frac{1}{2} \bar{t}_{ad}^{kl} (V_{ce}^{im}) \cdot \bar{t}_i^a \cdot \bar{t}_{kl}^{cd} - \frac{1}{2} \bar{t}_{cd}^{il} (V_{ae}^{km}) \cdot \bar{t}_i^a \cdot \bar{t}_{kl}^{cd} - \frac{1}{2} \bar{t}_{ed}^{kl} (V_{ca}^{mi}) \cdot \bar{t}_i^a \cdot \bar{t}_{kl}^{cd} \\ &- \frac{1}{2} \bar{t}_{cd}^{ml} (V_{ea}^{ki}) \cdot \bar{t}_i^a \cdot \bar{t}_{kl}^{cd} + \frac{1}{4} \bar{t}_{ae}^{lk} (V_{dc}^{im}) \cdot \bar{t}_i^a \cdot \bar{t}_{kl}^{cd} + \frac{1}{4} \bar{t}_{cd}^{mi} (V_{ae}^{lk}) \cdot \bar{t}_i^a \cdot \bar{t}_{kl}^{cd} \\ &- \bar{t}_{ed}^{il} (V_{ca}^{km}) \cdot \bar{t}_i^a \cdot \bar{t}_{kl}^{cd} - \bar{t}_{ad}^{ml} (V_{ce}^{ki}) \cdot \bar{t}_i^a \cdot \bar{t}_{kl}^{cd} \end{aligned}$$

$$\begin{aligned}
\left(G_{ef}^{XY}t\right)^{mn} &= -P_{-ef}\bar{t}_{ec}^{mn}(V_{fa}^{ki})\cdot t_i^x\cdot t_k^y - P_{-mn}\bar{t}_{ef}^{mk}(V_{ca}^{ni})\cdot t_i^x\cdot t_k^y \\
&\quad - P_{-ef}\bar{t}_{ea}^{mn}(V_{fc}^{ik})\cdot t_i^x\cdot t_k^y - P_{-mn}\bar{t}_{ef}^{mi}(V_{ac}^{nk})\cdot t_i^x\cdot t_k^y \\
&\quad + \bar{t}_{ef}^{ki}(V_{ca}^{mn})\cdot t_i^x\cdot t_k^y + \bar{t}_{ca}^{mn}(V_{ef}^{ki})\cdot t_i^x\cdot t_k^y \\
&\quad - P_{-mn}P_{-ef}\bar{t}_{fa}^{mk}(V_{ec}^{mi})\cdot t_i^x\cdot t_k^y - P_{-mn}P_{-ef}\bar{t}_{ec}^{mk}(V_{fa}^{nk})\cdot t_i^x\cdot t_k^y
\end{aligned} \tag{2}$$

where  $a, b, c, \dots$  indicate particle lines,  $i, j, k, \dots$  hole lines, and  $p, q, r, s, \dots$  general indexes,<sup>3</sup> and  $P_{pq}$  indicates a permutation operator, with  $: P_{pq}f(\dots pq \dots) = f(\dots pq \dots) - f(\dots qp \dots)$ . Furthermore,  $\bar{t}_q^p, \bar{t}_{rs}^{pq}$  denote the single and double ground-state Lagrange multipliers, and  $V_{rs}^{pq}$  an antisymmetrized two-electron integral.

## QR-EOMCC equations

Within the EOM-CC approximation, the quadratic response function is expressed below:<sup>4-6</sup>

$$\begin{aligned}
{}^{\text{EOM}}\langle\langle X; Y, Z \rangle\rangle_{\omega_Y, \omega_Z} &= \frac{1}{2}C^{\pm\omega}P^{X,Y,Z} \\
&\quad [- {}^{\text{EOM}}\bar{t}^X(\omega_X)^Y t(\omega_Y) \bar{t}^Z \xi^Z \\
&\quad + {}^{\text{EOM}}\bar{t}^X(\omega_X) {}^{\text{EOM}}\mathbf{A}^{YZ} t(\omega_Z) \\
&\quad - \bar{t}^Y(\omega_Y) {}^{\text{EOM}}\bar{t}^Z(\omega_Z) \xi^X]
\end{aligned} \tag{3}$$

where  $\bar{t}$  indicates the zeroth-order multipliers and  ${}^{\text{EOM}}\mathbf{A}^X$  is the EOM-CC property Jacobian matrix

$${}^{\text{EOM}}\mathbf{A}_{\mu\nu}^Y = \langle \mu | [\bar{Y}, |\nu\rangle \langle \text{HF} | ] | \text{HF} \rangle \tag{4}$$

$$\bar{Y} = e^{-\hat{T}} \hat{Y} e^{\hat{T}} \tag{5}$$

The EOM-CC right-hand side first order response equation is the same as the one pre-

sented in the manuscript, whereas the left-hand side first order response equation the  $\mathbf{F}t^Y$  term is replaced by  $\bar{t}_D \xi_S^Y + (\bar{t} \xi^Y) \bar{t}$ , yielding

$$\text{EOM}_t^Y(\bar{\mathbf{H}} + \omega_Y \mathbf{I}) = -\eta^X - \bar{t}_D \xi_S^Y + (\bar{t} \xi^Y) \bar{t}. \quad (6)$$

The subscripts "S" and "D" denote singles and doubles blocks, respectively.

# First hyperpolarizabilities of HX (X = F-Ts)

Table 1: QR-CCSD (CC) and QR-EOMCCSD (EOM) values for the  $\beta_{zxx}$  component (in a.u.) of the first hyperpolarizability of hydrogen halides, as well as their difference ( $\Delta\beta_{zxx}$ ). All calculations correlate eight (valence) electrons virtuals up to 5 a.u., except those marked by “\*”, in which all electrons and virtuals are correlated; †calculated with Dunning basis sets for the halogens; nc: not calculated.

Method	Hamiltonian	HF	HCl	HBr	HI	HAt	HTs
CC	LL	-1.6922	-0.6742	1.0636	3.7952	7.0220	25.5116
	LL†	-1.7528	-0.9107	0.9085	nc	nc	nc
	SF-X2C	-1.6937	-0.6120	1.7100	6.1264	20.1247	96.2015
	SF- <sup>2</sup> DC <sup>M</sup>	-1.6937	-0.6122	1.7086	6.1240	20.1191	96.3081
	X2C	-1.6939	-0.6125	1.7702	6.8921	29.8295	278.7012
	X2C†	-1.7547	-0.8486	1.6143	nc	nc	nc
	<sup>2</sup> DC <sup>M</sup>	-1.6939	-0.6111	1.7714	6.9246	30.2199	288.7374
	<sup>2</sup> DC <sup>M,*</sup>	-1.6121	-0.5613	1.7282	nc	nc	nc
	<sup>2</sup> DCG <sup>M</sup>	-1.6936	-0.6083	1.7840	6.9473	30.2659	288.1002
	EOM	LL	-1.4545	0.1867	2.8480	6.7308	11.1312
LL†		-1.5276	-0.0858	2.6604	nc	nc	nc
SF-X2C		-1.4550	0.2573	3.5540	9.2200	24.1946	93.8942
SF- <sup>2</sup> DC <sup>M</sup>		-1.4551	0.2570	3.5530	9.2194	24.1958	93.9776
X2C		-1.4552	0.2566	3.6077	9.8901	32.2297	245.9024
X2C†		-1.5286	-0.0157	3.4213	nc	nc	nc
<sup>2</sup> DC <sup>M</sup>		-1.4553	0.2581	3.6110	9.9316	32.6382	255.1885
<sup>2</sup> DC <sup>M,*</sup>		-1.4632	0.2319	3.2191	nc	nc	nc
<sup>2</sup> DCG <sup>M</sup>		-1.4555	0.2582	3.6116	9.9241	32.6553	254.9151
$\Delta\beta_{zxx}$		LL	-0.2377	-0.8609	-1.7844	-2.9356	-4.1092
	LL†	-0.2253	-0.8249	-1.7519	nc	nc	nc
	SF-X2C	-0.2386	-0.8693	-1.8440	-3.0935	-4.0698	2.3073
	SF- <sup>2</sup> DC <sup>M</sup>	-0.2386	-0.8692	-1.8445	-3.0954	-4.0768	2.3304
	X2C	-0.2386	-0.8691	-1.8375	-2.9980	-2.4002	32.7988
	X2C†	-0.2261	-0.8329	-1.8070	nc	nc	nc
	<sup>2</sup> DC <sup>M</sup>	-0.2386	-0.8692	-1.8395	-3.0070	-2.4183	33.5489
	<sup>2</sup> DC <sup>M,*</sup>	-0.1489	-0.7932	-1.4909	nc	nc	nc
	<sup>2</sup> DCG <sup>M</sup>	-0.2381	-0.8665	-1.8276	-2.9769	-2.3894	33.1851

Table 2: QR-CCSD (CC) and QR-EOMCCSD (EOM) values for the  $\beta_{zzz}$  component (in a.u.) of the first hyperpolarizability of hydrogen halides, as well as their difference ( $\Delta\beta_{zzz}$ ). All calculations correlate eight (valence) electrons virtuals up to 5 a.u., except those marked by “\*”, in which all electrons and virtuals are correlated; †calculated with Dunning basis sets for the halogens; nc: not calculated.

Method	Hamiltonian	HF	HCl	HBr	HI	HA <sub>t</sub>	HT <sub>s</sub>
CC	LL	-10.0225	-12.3576	-11.3099	-4.9920	2.5122	26.4008
	LL <sup>†</sup>	-9.8894	-12.8290	-11.6437	nc	nc	nc
	SF-X2C	-10.0265	-12.2467	-10.2951	-1.7249	19.1581	97.0937
	SF- <sup>2</sup> DC <sup>M</sup>	-10.0265	-12.2457	-10.2927	-1.7207	19.1714	97.2916
	X2C	-10.0351	-12.2800	-10.7858	-4.1339	6.2096	236.5265
	X2C <sup>†</sup>	-9.8918	-12.7406	-11.0795	nc	nc	nc
	<sup>2</sup> DC <sup>M</sup>	-10.0285	-12.2682	-10.7667	-4.2923	5.8862	247.7845
	<sup>2</sup> DC <sup>M,*</sup>	-9.9662	-12.3004	-11.3303	nc	nc	nc
	<sup>2</sup> DCC <sup>M</sup>	-10.0285	-12.2698	-10.7700	-4.2988	5.8167	246.5360
	EOM	LL	-9.5863	-9.7123	-6.1185	5.1071	16.9523
LL <sup>†</sup>		-9.4973	-10.2439	-6.4784	nc	nc	nc
SF-X2C		-9.5887	-9.5979	-5.1513	7.7038	29.0053	85.6894
SF- <sup>2</sup> DC <sup>M</sup>		-9.5887	-9.5976	-5.1508	7.7011	28.9897	85.6045
X2C		-9.5972	-9.6318	-5.6680	4.9753	11.4539	184.6568
X2C <sup>†</sup>		-9.4983	-10.1522	-5.9790	nc	nc	nc
<sup>2</sup> DC <sup>M</sup>		-9.5908	-9.6206	-5.6478	4.8241	11.1031	194.7558
<sup>2</sup> DC <sup>M,*</sup>		-9.7486	-9.8647	-7.1271	nc	nc	nc
<sup>2</sup> DCC <sup>M</sup>		-9.5917	-9.6261	-5.6664	4.7873	11.0986	194.7453
$\Delta\beta_{zzz}$		LL	-0.4362	-2.6452	-5.1914	-10.0991	-14.4401
	LL <sup>†</sup>	-0.3920	-2.5851	-5.1653	nc	nc	nc
	SF-X2C	-0.4378	-2.6488	-5.1438	-9.4287	-9.8472	11.4044
	SF- <sup>2</sup> DC <sup>M</sup>	-0.4377	-2.6481	-5.1419	-9.4218	-9.8182	11.6871
	X2C	-0.4379	-2.6482	-5.1179	-9.1092	-5.2443	51.8697
	X2C <sup>†</sup>	-0.3935	-2.5884	-5.1005	nc	nc	nc
	<sup>2</sup> DC <sup>M</sup>	-0.4377	-2.6476	-5.1189	-9.1163	-5.2169	53.0287
	<sup>2</sup> DC <sup>M,*</sup>	-0.2176	-2.4356	-4.2032	nc	nc	nc
	<sup>2</sup> DCC <sup>M</sup>	-0.4368	-2.6437	-5.1036	-9.0861	-5.2818	51.7907

Table 3: Breakdown of the contributions (in a.u.) from each of the terms in eq. 1 to the static QR-CCSD response functions  $\langle\langle X; Y, Z \rangle\rangle_0$ , (after all permutations) for the calculations with the  ${}^2\text{DC}^M$  Hamiltonian and correlating eight (valence) electrons virtuals up to 5 a.u. . The column “singles” (“doubles”) denote the contributions from the contraction between the singles(doubles) block of the terms in square brackets and the  $\overset{z}{t}$  tensor. The column “total” correspond to the sum of the “singles” and “doubles” contributions.

System	Term	$\langle\langle Z; Z, Z \rangle\rangle_0$			$\langle\langle Z; X, X \rangle\rangle_0$		
		total	singles	doubles	total	singles	doubles
HF	$\mathbf{F}^{X\overset{Y}{t}}(\omega_Y)\overset{Z}{t}(\omega_Z)$	-0.5139	-0.2901	-0.2238	-0.0748	-0.0458	-0.0290
	$\mathbf{G}^{\overset{x}{t}}(\omega_X)\overset{Y}{t}(\omega_Y)\overset{Z}{t}(\omega_Z)$	-0.0513	-0.0698	0.0185	0.0011	-0.0017	0.0028
	$\overset{x}{t}(\omega_X)\mathbf{B}^{\overset{Y}{t}}(\omega_Y)\overset{Z}{t}(\omega_Z)$	-3.1113	-3.0875	-0.0238	-0.9085	-0.9718	0.0634
	$\overset{x}{t}(\omega_X)\mathbf{A}^{Y\overset{Z}{t}}(\omega_Z)$	13.7050	15.3507	-1.6457	2.6761	3.2016	-0.5255
	sum	10.0285	11.9034	-1.8749	1.6939	2.1823	-0.4884
HCl	$\mathbf{F}^{X\overset{Y}{t}}(\omega_Y)\overset{Z}{t}(\omega_Z)$	-1.2492	-0.7032	-0.5460	-0.3202	-0.2411	-0.0791
	$\mathbf{G}^{\overset{x}{t}}(\omega_X)\overset{Y}{t}(\omega_Y)\overset{Z}{t}(\omega_Z)$	-0.0845	-0.1599	0.0754	0.0442	0.0353	0.0088
	$\overset{x}{t}(\omega_X)\mathbf{B}^{\overset{Y}{t}}(\omega_Y)\overset{Z}{t}(\omega_Z)$	-6.3625	-6.7142	0.3517	-2.6790	-2.9266	0.2476
	$\overset{x}{t}(\omega_X)\mathbf{A}^{Y\overset{Z}{t}}(\omega_Z)$	19.9643	25.0924	-5.1281	3.5662	5.4898	-1.9235
	sum	12.2682	17.5151	-5.2469	0.6111	2.3573	-1.7462
HBr	$\mathbf{F}^{X\overset{Y}{t}}(\omega_Y)\overset{Z}{t}(\omega_Z)$	-1.9007	-1.0708	-0.8299	-0.5289	-0.4014	-0.1275
	$\mathbf{G}^{\overset{x}{t}}(\omega_X)\overset{Y}{t}(\omega_Y)\overset{Z}{t}(\omega_Z)$	-0.0834	-0.2054	0.1219	0.0779	0.0622	0.0157
	$\overset{x}{t}(\omega_X)\mathbf{B}^{\overset{Y}{t}}(\omega_Y)\overset{Z}{t}(\omega_Z)$	-7.7564	-7.9359	0.1794	-4.1734	-4.5494	0.3759
	$\overset{x}{t}(\omega_X)\mathbf{A}^{Y\overset{Z}{t}}(\omega_Z)$	20.5073	26.9694	-6.4621	2.8530	6.1112	-3.2582
	sum	10.7667	17.7573	-6.9906	-1.7714	1.2225	-2.9940
HI	$\mathbf{F}^{X\overset{Y}{t}}(\omega_Y)\overset{Z}{t}(\omega_Z)$	-1.9820	-1.1233	-0.8587	-0.9588	-0.7776	-0.1812
	$\mathbf{G}^{\overset{x}{t}}(\omega_X)\overset{Y}{t}(\omega_Y)\overset{Z}{t}(\omega_Z)$	-0.0214	-0.1844	0.1630	0.1575	0.1370	0.0205
	$\overset{x}{t}(\omega_X)\mathbf{B}^{\overset{Y}{t}}(\omega_Y)\overset{Z}{t}(\omega_Z)$	-7.0690	-6.8321	-0.2369	-6.3643	-6.8736	0.5093
	$\overset{x}{t}(\omega_X)\mathbf{A}^{Y\overset{Z}{t}}(\omega_Z)$	13.3647	19.4919	-6.1272	0.2410	5.1993	-4.9583
	sum	4.2923	11.3520	-7.0597	-6.9246	-2.3150	-4.6096

Table 4: Breakdown of the contributions (in a.u.) from each of the terms in eq. 3 to the static QR-EOMCCSD response functions  $\langle\langle X; Y, Z \rangle\rangle_0$ , (after all permutations) for the calculations with the  ${}^2\text{DC}^M$  Hamiltonian and correlating eight (valence) electrons virtuals up to 5 a.u.. The column “singles” (“doubles”) denote the contributions from the contraction between the singles(doubles) block of the  $[\text{EOM}_\eta^X \mathbf{A}^Y]$  and  $\overset{Z}{t}$  tensors. The column “total” correspond to the sum of the “singles” and “doubles” contributions, plus the ”sd+ds” column, which corresponds to the cross-terms arising from the 4-tensor products ( $[-\overset{XY}{\bar{t}t}][\bar{t}\xi^Z]$  and  $-\overset{Y}{\bar{t}t}[\bar{t}\xi^X]$ ).

System	Term	$\langle\langle Z; Z, Z \rangle\rangle_0$				$\langle\langle Z; X, X \rangle\rangle_0$			
		total	singles	doubles	sd+ds	total	singles	doubles	sd+sd
HF	$-\overset{XY}{\bar{t}t\bar{t}}\xi^Z$	-0.7616	-0.2959	-0.0249	-0.4407	-0.2216	-0.0860	-0.0074	-0.1282
	$\text{EOM}_\eta^X \mathbf{A}^Y \overset{Z}{t}$	11.0952	13.1353	-2.0401	0.0000	1.8815	2.4852	-0.6037	0.0000
	$-\overset{YZ}{\bar{t}t\bar{t}}\xi^X$	-0.7429	-0.2827	-0.0218	-0.4384	-0.2046	-0.0780	-0.0058	-0.1208
	sum	9.5908	12.5567	-2.0868	-0.8791	1.4553	2.3212	-0.6168	-0.2490
HCl	$-\overset{XY}{\bar{t}t\bar{t}^0}\xi^Z$	-2.3768	-1.3300	-0.0495	-0.9962	-0.7690	-0.4307	-0.0160	-0.3223
	$\text{EOM}_\eta^X \mathbf{A}^Y \overset{Z}{t}$	14.6500	21.2000	-6.5375	0.0000	1.3102	3.4600	-2.1498	0.0000
	$-\overset{YZ}{\bar{t}t\bar{t}}\xi^X$	-2.6526	-1.3700	-0.0607	-1.2181	-0.7992	-0.4150	-0.0174	-0.3668
	sum	9.6206	18.5000	-6.6477	-2.2143	-0.2581	2.6144	-2.1833	-0.6892
HBr	$-\overset{XY}{\bar{t}t\bar{t}}\xi^Z$	-4.0194	-2.1189	-0.0887	-1.8118	-1.3421	-0.7077	-0.0295	-0.6049
	$\text{EOM}_\eta^X \mathbf{A}^Y \overset{Z}{t}$	13.9372	22.4470	-8.5098	0.0000	-0.9642	2.6929	-3.4997	0.0000
	$-\overset{YZ}{\bar{t}t\bar{t}}\xi^X$	-4.2700	-2.1914	-0.0980	-1.9806	-1.3046	-0.6717	-0.0281	-0.6048
	sum	5.6478	18.1367	-8.6965	-3.7923	-3.6110	1.3135	-3.5573	-1.2097
HI	$-\overset{XY}{\bar{t}t\bar{t}}\xi^Z$	-6.6787	-3.5975	-0.1503	-2.9309	-2.2608	-1.2200	-0.0492	-0.9916
	$\text{EOM}_\eta^X \mathbf{A}^Y \overset{Z}{t}$	8.4536	17.1299	-8.6763	0.0000	-5.6300	-0.1012	-5.5288	-0.0000
	$-\overset{YZ}{\bar{t}t\bar{t}}\xi^X$	-6.5990	-3.8031	-0.1373	-2.6586	-2.0407	-1.1815	-0.0390	-0.8203
	sum	-4.8241	9.7293	-8.9639	-5.5895	-9.9316	-2.5026	-5.6171	-1.8119

# Polarizabilities of HX (X = F-Ts) and noble gas atoms

Table 5: CCSD equilibrium dipole moment ( $\mu_z$ ) and static dipole polarizabilities for hydrogen halides obtained with the symmetric (CC) and asymmetric (aCC) formulations of LR-CCSD, and LR-EOMCCSD (EOM). Apart from components ( $\alpha_{zz}, \alpha_{xx}$ ) we report the mean values and the anisotropy ( $\bar{\alpha} = (\alpha_{zz} + 2\alpha_{xx})/3$ ).  $\Delta = \alpha^{\text{CC}} - \alpha^{\text{EOM}}$  denotes the difference between properties calculated with CC and EOM. All calculations correlate eight (valence) electrons virtuals up to 5 a.u., and all values are given in a.u.; The experimental dipole moment values<sup>7</sup> correspond to  $\mu_0$  instead of the equilibrium values obtained from the calculations.

Property	Method	HF	HCl	HBr	HI	HA <sub>t</sub>	HT <sub>s</sub>
$\mu_z$	CC	0.6916	0.4229	0.3011	0.1499	-0.0880	-0.7989
	Exp. <sup>7</sup> CCSD(T) <sup>8</sup>	0.7186	0.4362	0.3254	0.1762		-0.7644
$\alpha_{zz}$	CC	6.5763	18.6242	25.5904	38.0011	46.5183	70.1581
	CC asym	6.5763	18.6242	25.5904	38.0011	46.5183	70.1581
	EOM	6.6476	18.9614	26.0809	38.8239	47.4742	71.5697
	$\Delta$	-0.0713	-0.3372	-0.4905	-0.8228	-0.9559	-1.4116
$\alpha_{xx}$	CC	5.4560	16.9257	23.5976	35.4944	43.5843	71.5091
	CC asym	5.4560	16.9257	23.5976	35.4944	43.5843	71.5091
	EOM	5.4924	17.1394	23.9058	36.0189	44.1797	72.4536
	$\Delta$	-0.0364	-0.2137	-0.3082	-0.5244	-0.5954	-0.9445
$\bar{\alpha}$	CC	5.8295	17.4919	24.2619	36.3300	44.5623	71.0588
	CC asym	5.8295	17.4919	24.2619	36.3300	44.5623	71.0588
	EOM	5.8775	17.7467	24.6308	36.9539	45.2779	72.1590
	$\Delta$	-0.0480	-0.2548	-0.3690	-0.6239	-0.7156	-1.1002
	Exp. <sup>9</sup>	5.6±0.1	17.4±0.01	23.79±0.5	37.1±0.5		
$\Delta\alpha$	CC	1.1203	1.6985	1.9928	2.5067	2.9340	-1.3510
	CC asym	1.1203	1.6984	1.9929	2.5066	2.9340	-1.3510
	EOM	1.1551	1.8220	2.1751	2.8051	3.2946	-0.8839
	$\Delta$	-0.0349	-0.1235	-0.1823	-0.2984	-0.3605	-0.4671

Table 6: Static and dynamic dipole polarizabilities ( $\alpha(\omega)$ , in a.u.) for noble gases obtained with the symmetric (CC) formulation of LR-CCSD and LR-EOMCCSD (EOM).  $\Delta = \alpha^{\text{CC}} - \alpha^{\text{EOM}}$  denotes the difference between properties calculated with CC and EOM. All calculations correlate 8 (*nsnp*) or 18 (*(n-1)dnsnp*) electrons virtuals up to 5 a.u.

Atom	$\omega$	<i>nsnp</i>			<i>(n - 1)dnsnp</i>		
		CC	EOM	$\Delta$	CC	EOM	$\Delta$
Xe	0.0000	28.1736	28.5905	-0.4169	27.9533	28.3785	-0.4253
	0.0100	28.1876	28.6047	-0.4171	27.9670	28.3924	-0.4254
	0.0200	28.2297	28.6473	-0.4176	28.0083	28.4342	-0.4260
	0.0300	28.3003	28.7187	-0.4185	28.0774	28.5043	-0.4268
	0.0428	28.4333	28.8534	-0.4201	28.2078	28.6363	-0.4285
	0.0500	28.5293	28.9505	-0.4212	28.3019	28.7315	-0.4296
	0.0656	28.7939	29.2184	-0.4244	28.5612	28.9941	-0.4329
	0.0774	29.0457	29.4732	-0.4274	28.8079	29.2439	-0.4359
	0.0900	29.3720	29.8033	-0.4313	29.1275	29.5674	-0.4399
Rn	0.0000	36.4840	37.0015	-0.5175	36.1210	36.6936	-0.5725
	0.0100	36.5100	37.0278	-0.5178	36.1461	36.7190	-0.5729
	0.0200	36.5883	37.1070	-0.5187	36.2217	36.7956	-0.5739
	0.0300	36.7199	37.2401	-0.5202	36.3487	36.9243	-0.5755
	0.0428	36.9695	37.4925	-0.5230	36.5896	37.1682	-0.5787
	0.0500	37.1506	37.6756	-0.5250	36.7644	37.3453	-0.5809
	0.0656	37.6553	38.1860	-0.5307	37.2512	37.8384	-0.5872
	0.0774	38.1426	38.6787	-0.5360	37.7211	38.3144	-0.5933
	0.0900	38.7851	39.3282	-0.5431	38.3403	38.9415	-0.6012
Og	0.0000	62.3732	64.9005	-2.5273	60.4439	61.4848	-1.0409
	0.0100	62.4796	65.0665	-2.5869	60.5419	61.5844	-1.0424
	0.0200	62.8024	65.4570	-2.6546	60.8392	61.8861	-1.0469
	0.0300	63.3526	66.0841	-2.7315	61.3456	62.4002	-1.0546
	0.0428	64.4241	67.2700	-2.8459	62.3302	63.3996	-1.0695
	0.0500	65.2263	68.1455	-2.9192	63.0659	64.1465	-1.0805
	0.0656	67.5821	70.6899	-3.1079	65.2194	66.3321	-1.1127
	0.0774	70.0500	73.3341	-3.2841	67.4630	68.6090	-1.1460
	0.0900	73.6588	77.1808	-3.5221	70.7189	71.9126	-1.1937

# Verdet constants for Xe, Rn and Og

Table 7: Verdet Constant  $V(\omega)$  [in  $10^{-3}$  rad/(T m)] for Gaseous Xe, Rn and Og at Different Laser Wavelengths, calculated with QR-CCSD (denoted by CC) and QR-EOMCCSD (denoted by EOM) upon correlating the  $(n-1)dnsnp$  shells (and with virtual threshold at 5 a.u.), as well as the difference in Verdet constant between the two approaches ( $\Delta V = V^{\text{CC}} - V^{\text{EOM}}$ ).

Atom	Hamiltonian	$\lambda(589 \text{ nm})$			$\lambda(694.3 \text{ nm})$			$\lambda(1064 \text{ nm})$		
		CC	EOM	$\Delta V$	CC	EOM	$\Delta V$	CC	EOM	$\Delta V$
Xe	SF-X2C	12.39	12.54	-0.15	8.72	8.82	-0.11	3.60	3.64	-0.04
	SF- <sup>2</sup> DC <sup>M</sup>	12.40	12.55	-0.15	8.72	8.83	-0.11	3.60	3.64	-0.04
	X2C	12.95	13.10	-0.15	9.10	9.20	-0.11	3.74	3.79	-0.05
	<sup>2</sup> DC <sup>M</sup>	13.00	13.16	-0.15	9.14	9.24	-0.11	3.76	3.81	-0.05
	<sup>2</sup> DCG <sup>M</sup>	12.97	13.12	-0.15	9.11	9.22	-0.11	3.75	3.80	-0.05
Rn	SF-X2C	18.79	19.01	-0.22	13.14	13.30	-0.15	5.38	5.44	-0.06
	SF- <sup>2</sup> DC <sup>M</sup>	18.82	19.04	-0.22	13.16	13.31	-0.15	5.38	5.45	-0.06
	X2C	25.62	25.90	-0.28	17.73	17.92	-0.19	7.14	7.22	-0.08
	<sup>2</sup> DC <sup>M</sup>	26.07	26.35	-0.28	18.03	18.22	-0.20	7.26	7.34	-0.08
	<sup>2</sup> DCG <sup>M</sup>	25.95	26.24	-0.28	17.95	18.15	-0.20	7.23	7.31	-0.08
Og	SF-X2C	35.45	35.83	-0.38	24.44	24.71	-0.27	9.81	9.91	-0.11
	SF- <sup>2</sup> DC <sup>M</sup>	35.58	35.95	-0.38	24.53	24.79	-0.26	9.84	9.95	-0.11
	X2C	144.66	146.52	-1.85	92.02	93.20	-1.18	33.34	33.77	-0.43
	<sup>2</sup> DC <sup>M</sup>	151.00	152.95	-1.95	95.74	96.98	-1.24	34.55	35.00	-0.45
	<sup>2</sup> DCG <sup>M</sup>	149.96	151.92	-1.96	95.12	96.36	-1.24	34.34	34.79	-0.45

# Excitation energies for Xe, Rn and Og

Table 8: Excitation energies for the some of the lowest-lying electronic states for Xe, Rn and Og, upon correlating the (a)  $nsnp$  and (b)  $(n-1)dnsnp$  electrons and virtuals up to 5 a.u. A comparison to the experimental data from NIST<sup>10</sup> is provided for Xe and Rn, with  $\Delta E$  values indicating the difference between our calculations and experiment.

	$\Omega$	E (eV)(a)	E (eV)(b)	Exp. <sup>10</sup>		config.	$\Delta E(a)$ (eV)	$\Delta E(b)$ (eV)
				J	E (eV)			
Xe	0g	0.000	0.000	0	0.000	$5p^6$		
	2u	8.076	8.101	2	8.315	$5p^5(^2P_{3/2})6s$	-0.239	-0.214
	1u	8.211	8.237	1	8.437	$5p^5(^2P_{3/2})6s$	-0.225	-0.199
	0u	9.192	9.240	0	9.447	$5p^5(^2P_{1/2})6s$	-0.255	-0.208
	1u	9.323	9.372	1	9.570	$5p^5(^2P_{1/2})6s$	-0.247	-0.198
	1g	9.313	9.339	1	9.580	$5p^5(^2P_{3/2})6p$	-0.267	-0.242
	2g	9.435	9.461	2	9.686	$5p^5(^2P_{3/2})6p$	-0.251	-0.225
	3g	9.464	9.492	3	9.721	$5p^5(^2P_{3/2})6p$	-0.257	-0.229
	1g	9.538	9.565	1	9.789	$5p^5(^2P_{3/2})6p$	-0.252	-0.224
	2g	9.569	9.596	2	9.821	$5p^5(^2P_{3/2})6p$	-0.253	-0.225
Rn	0g	0.000	0.000	0	0.000	$6p^6$		
	2u	6.542	6.575	2	6.772	$6p^5(^2P_{3/2})7s$	-0.230	-0.197
	1u	6.724	6.763	1	6.942	$6p^5(^2P_{3/2})7s$	-0.217	-0.179
	1g	7.948	8.024	1	8.213	$6p^5(^2P_{3/2})7p$	-0.265	-0.189
	2g	8.017	8.096	2	8.271	$6p^5(^2P_{3/2})7p$	-0.253	-0.175
	0u	8.179	8.259	0	8.419	$6p^5(^2P_{3/2})6d$	-0.240	-0.161
	3g	8.170	8.245	3	8.436	$6p^5(^2P_{3/2})7p$	-0.266	-0.191
	1g	8.211	8.287	1	8.472	$6p^5(^2P_{3/2})7p$	-0.262	-0.185
	2g	8.268	8.345	2	8.529	$6p^5(^2P_{3/2})7p$	-0.260	-0.183
	1u	8.305	8.386	1	8.541	$6p^5(^2P_{3/2})6d$	-0.236	-0.155
Og	0g	0.000	0.000					
	2u	3.996	4.068					
	1u	4.383	4.466					
	1g	5.841	5.971					
	2g	5.879	6.012					
	0u	6.392	6.502					
	3g	6.397	6.515					
	1g	6.410	6.529					

## Sample timings for quadratic response evaluation

Table 9: Comparison of timings for the quadratic response evaluation step for the  $\beta_{zzz}$  component of the dipole hyperpolarizability (wall time, in hh:mm:ss format) between for QR-CC and QR-EOMCC, and the ratio between them. Calculations with the  ${}^2\text{DC}^M$  Hamiltonian. O: number of correlated electrons, V: number of virtual spinors. QRF: quadratic response function evaluation step; total: all steps (QR, solution of linear systems etc.)

system	O	V	Method	total walltime	ratio	QRF walltime <sup>†</sup>
valence electrons correlated						
HF	8	196	CC	0:34:07		0:13:51
			EOMCC	0:18:51	0.6	0:00:12
HCl	8	226	CC	0:37:37		0:21:36
			EOMCC	0:16:18	0.4	0:00:06
HBr	8	226	CC	1:05:55		0:26:31
			EOMCC	0:39:35	0.6	0:00:08
all electrons correlated						
HF	10	282	CC	0:57:44		0:17:31
			EOMCC	0:41:06	0.7	0:00:11
HCl	18	300	CC	1:56:59		0:28:44
			EOMCC	1:32:24	0.8	0:00:33
HBr	36	402	CC	8:36:03		2:24:50
			EOMCC	6:14:54	0.7	0:02:36

## References

- (1) Christiansen, O.; Jørgensen, P.; Hättig, C. Response functions from Fourier component variational perturbation theory applied to a time-averaged quasienergy. *Int. J. Quantum. Chem* **1998**, *68*, 1–52.
- (2) Yuan, X.; Halbert, L.; Pototschnig, J. V.; Papadopoulos, A.; Coriani, S.; Visscher, L.; Pereira Gomes, A. S. Formulation and Implementation of Frequency-Dependent Linear Response Properties with Relativistic Coupled Cluster Theory for GPU-Accelerated Computer Architectures. *Journal of Chemical Theory and Computation* **2024**, *20*, 677–694.
- (3) Crawford, T. D.; Schaefer III, H. F. An introduction to coupled cluster theory for computational chemists. *Rev. comp. chem* **2007**, *14*, 33–136.
- (4) Pawłowski, F.; Olsen, J.; Jørgensen, P. Molecular response properties from a Hermitian eigenvalue equation for a time-periodic Hamiltonian. *J. Chem. Phys* **2015**, *142*, 114109.
- (5) Coriani, S.; Pawłowski, F.; Olsen, J.; Jørgensen, P. Molecular response properties in equation of motion coupled cluster theory: A time-dependent perspective. *J. Chem. Phys* **2016**, *144*, 024102.
- (6) Faber, R.; Coriani, S. Resonant inelastic X-ray scattering and nonresonant X-ray emission spectra from coupled-cluster (damped) response theory. *J. Chem. Theory. Comput* **2018**, *15*, 520–528.
- (7) Lovas, F. *Diatom Spectral Database, NIST Standard Reference Database 114*; National Institute of Standards and Technology, 2002.
- (8) Thierfelder, C.; Schwerdtfeger, P.; Koers, A.; Borschevsky, A.; Fricke, B. Scalar relativistic and spin-orbit effects in closed-shell superheavy-element monohydrides. *Phys. Rev. A* **2009**, *80*, 022501.

- (9) Hohm, U. Experimental static dipole–dipole polarizabilities of molecules. *Journal of Molecular Structure* **2013**, *1054–1055*, 282–292.
- (10) Kramida, A.; Ralchenko, Y. NIST Atomic Spectra Database, NIST Standard Reference Database 78. 1999; <http://www.nist.gov/pml/data/asd.cfm>.